FINITE ELEMENT AND EQUIVALENT CIRCUIT MODELING OF CAPACITIVE MICROMACHINED ULTRASONIC TRANSDUCER (CMUT)

by

F. Yalçın YAMANER

Submitted to the Graduate School of Engineering and Natural Sciences
in partial fulfillment of
the requirements for the degree of
Master of Science

SABANCI UNIVERSITY
Summer 2006

to my dear parents for their support

FINITE ELEMENT AND EQUIVALENT CIRCUIT MODELING OF CAPACITIVE MICROMACHINED ULTRASONIC TRANSDUCER (CMUT)

APPROVED BY

Assist. Prof. Dr. Ayhan BOZKURT ………………….

(Dissertation Supervisor)

Assoc. Prof. Dr. Yaşar GÜRBÜZ ………………….

Assist. Prof. Dr. Serhat YEŞİLYURT ………………..…

Assist. Prof. Dr. Cem ÖZTÜRK ………………..…

Assist. Prof. Dr. Güllü Kızıltaş ŞENDUR ………………….

DATE OF APPROVAL: ………………………….

© F. Yalçın Yamaner 2006

All Rights Reserved

FINITE ELEMENT AND EQUIVALENT CIRCUIT MODELING OF CAPACITIVE MICROMACHINED ULTRASONIC TRANSDUCER (CMUT)

F. Yalçın Yamaner

EECS, MSc Thesis, 2006

Thesis Supervisor: Assist. Prof. Dr. Ayhan BOZKURT

Keywords: Capacitive micromachined ultrasonic transducer (CMUT), finite element model (FEM), Mason model, immersed CMUT

Abstract

In this thesis, a precise finite element model (FEM) of capacitive micromachined ultrasonic transducer is developed. Trough the results of the FEM, an equivalent circuit model of a transducer is built which enables high efficient design of transceiver front-end integrated circuit with a better known transducer behavior. Consequently, more realistic simulation results of the overall system can be obtained. The FEM model is created in the ANSYS environment and all simulations are done in 3D. The model can also be used to determine the proper parameters (e.g. radius, thickness, gap height) for the target of operation without fabrication. The equivalent circuit that is constructed over the Mason model is improved for immersion applications with modeling the radiation impedance with an RLC circuit and defining an effective transformer ratio value. Modeling results match actual measurements with a very good accuracy.

SİLİKON MİKROİŞLEME YÖNTEMİYLE ÜRETİLEN KAPASİTİF ULTRASONİK DÖNÜŞTÜRÜCÜLERİN (CMUT) SONLU ELEMAN ve EŞDEĞER DEVRE MODELİ

F. Yalçın Yamaner

EECS, Yüksek Lisans Tezi, 2006

Tez Danışmanı: Yard. Doç. Dr. Ayhan BOZKURT

Anahtar Kelimeler: Silikon mikroişleme yöntemiyle üretilen kapasitif ultrasonik dönüştürücü (CMUT), sonlu eleman modeli (FEM), Mason modeli, daldırılmış CMUT

Özet

Bu tezde, silikon mikroişleme yöntemiyle üretilen kapasitif ultrasonik dönüştürücülerin (CMUT) sonlu eleman metodu (FEM) kullanılarak gerçekçi bir modeli oluşturulmuştur. Oluşturulan bu modelin sonuçları doğrultusunda dönüştürücünün eşdeğer devre modeli geliştirilmiştir. Bu devre, dönüştürünün elektriksel eşdeğerini ortaya koyduğundan, daha verimli ön/alıcı verici tümleşik devrelerinin dizayn edilmesine olanak sağlamaktadır. Sonuç olarak, tüm sistemin daha gerçekçi simulasyon sonuçları elde edilebilmektedir. Sonlu eleman modeli ANSYS ortamında oluşturulmuş ve simulasyonlar üç boyutta yapılmıştır. Bu model kullanılarak, hedeflenen uygulama için üretim öncesi dönüştürücü parametreleri (zar yarıçapı, zar kalınlığı, hücrelerin silikon taban üzerindeki dağılımları) belirlenebilmekte ve üzerlerinde iyileştirmeler yapılabilmektedir. Mason modeli temel alınarak oluşturulan eşdeğer devre, dönüştürücü katsayısı iyileştirilerek ve radyasyon empedansı RLC devresi ile modellenerek geliştirilmiştir. Model sonuçları gerçek ölçümlerle oldukça uyumludur.

Acknowledgements

I wish to express my deepest gratitude to my supervisor Ayhan Bozkurt for his valuable advice and guidance of this work. I am grateful to him not only for the completion of this thesis, but also for his unconditional support. I could not complete this difficult process without his advisement, enthusiasm and friendly support.

I am grateful to my thesis committee members Yaşar GÜRBÜZ, Serhat YEŞİLYURT, Cem ÖZTÜRK and, Güllü Kızıltaş ŞENDUR for their valuable review and comments on the thesis.

Special thanks to my colleagues in the department and to our lab responsible, Bulent KÖROGLU. They have shared their knowledge, experience with me, which have made my life and study at Sabanci University easier and more enjoyable.

I would like to thank all my friends for their friendship and endless support.

Lastly, I would like to thank my family for their endless love and patience. Their limitless tolerance made everything about me possible. I dedicate this work to my family.

TABLE OF CONTENTS

ABSTRACT V
ÖZET VI
1 INTRODUCTION 1
2 FUNDAMENTALS: CMUT 3
2.1 CMUT Structure 3
2.2 Operating Principle 5
2.3 First Order Model 5
2.4 Electrical Equivalent Circuit Model 9
2.4.1 Mechanical Impedance of the Membrane: Z_{mem} 9
2.4.2 Device Capacitance: C_0 11
2.4.3 Transformer Ratio: n 12
2.4.4 Spring Softening Capacitor: $-C_0/n^2$ 13
2.4.5 Parasitic Capacitor: C_p 14
2.4.6 Radiation Impedance of the membrane: Z_{rad} 14
3 FINITE ELEMENT MODEL 15
3.1 ANSYS Model 15
3.2 Static Analysis 18
3.3 Modal Analysis 20
3.4 Harmonic Analysis 21
3.5 Membrane Mechanical Impedance 22
3.7 Immersed Operation 27
3.8 Transient Analysis 33
3.9 Array Operation 34
4 MEASUREMENTS 37
4.1 Impedance Measurements 38
4.2 Hydrophone Measurements 41
4.3 Pulse Echo Measurements 45

4.4 Equivalent circuit model of the fabricated CMUT element 49
5 CONCLUSION AND FUTURE WORK 53
BIBLIOGRAPHY 54
APPENDIX A 55
FABRICATION OF CMUTS 56
A.1 Conventional Method: Sacrificial Layer 56
A.1.1 Vacuum Sealing 58
A.1.2 Metallization 59
A.2 Wafer Bonding Method 59
A.2.1 Vacuum Cavity Formation 60
A.2.2 Cavity Size and Shape 60
A.2.3 Membrane Material 60
A.2.4 Fill Factor 61
A.2.5 Fabrication Process 61

LIST OF FIGURES

Figure 2.1 : Cross sectional view of a CMUT cell 3
Figure 2.2 : 3D visualization of a CMUT 2D array element 4
Figure 2.3 : Lumped first order model of a CMUT 6
Figure 2.4 : Electrical equivalent circuit of a CMUT 9
Figure 2.5 : Equivalent circuit representation of membrane impedance for the first harmonic excitation... 11
Figure 3.6 : Average displacement over the membrane 21
Figure 3.7 : Membrane impedance (R=15μm, t_m=1.2, t_g=0.2). Ansys results fit the theoretical results. 23
Figure 3.8 : Membrane impedance. LC circuit models the membrane impedance with a high accuracy where L=5.19pH and C=8.17μF.. 23
Figure 3.9 : Transformer ratio versus bias voltage. 25
Figure 3.10 : Equivalent circuit model of a single air coupled CMUT 26
Figure 3.11 : Input Impedance comparison between equivalent circuit model and FEM for membrane geometry in Figure 3.3. 26
Figure 3.12 : Input impedance using improved circuit model and FEM 27
Figure 3.13 : Meshed model of immersed CMUT.. 28
Figure 3.14 : Average displacement of the membrane in two different environments.. 29
Figure 3.15 : Single cell surface pressure in water at a resonant frequency of 11 MHz 29
Figure 3.16 : Surface average pressure (harmonic and transient analysis comparison) 30
Figure 3.17 : Radiation impedance of a single CMUT cell 31
Figure 3.18 : Parallel RLC circuit model optimized for the radiation impedance found using MATLAB.. 31
Figure 3.19 : Equivalent circuit model of a single immersion CMUT 32

Figure 3.20 : Real part of input impedance of circuit shown in Figure 3.19. 32
Figure 3.21 : Imaginary part of input impedance of circuit shown in Figure 3.19.33
Figure 3.22 : An example of 1D (a) and 2D (b) arrays.. 34
Figure 3.23 : Hexagonal array, 3x3 array and, 4x4 array after a static analysis of 128V DC bias.. 35
Figure 3.24 : Average pressure over the surface of arrays obtained by using ANSYS 36
Figure 3.25 : 3dB fractional bandwidth comparison over ANSYS results............ 36
Figure 4.1 : 5x5 CMUT array fabricated using conventional method.................. 37
Figure 4.2 : Real and imaginary part of the input impedance of 4x4 CMUT array with no dc bias 39
Figure 4.3 : Real part of the input impedance of 4x4 CMUT array at various bias voltages. 40
Figure 4.4 : Imaginary part of the input impedance of 4x4 CMUT array at various bias voltages... 40
Figure 4.5 : Input capacitance under 30 volt DC bias 41
Figure 4.6 : Applied input pulse in the experiments.. 42
Figure 4.7 : Hydrophone measurement at a distance of 8 mm from the array surface 43
Figure 4.8 : Detected pressure signal at 8mm distance from array surface 43
Figure 4.9 : Fourier transform of the detected pressure signal 44
Figure 4.10: Pressure signal at a distance of from the transducer surface (FEM). Same pulse signal used as in experimental input.. 44
Figure 4.11: FEM analyses results are compared with experimental data in terms of pressure... 45
Figure 4.12: Experimental pulse-echo setup... 46
Figure 4.13: Schematic setup for pulse echo measurements. 47
Figure 4.14: Pulse echo response... 47
Figure 4.15: Detected echo signal... 48
Figure 4.16: Bandwidth of the detected echo signal.. 48
Figure 4.17: Illustration of equivalent circuit model of a CMUT element with N cell.. 49
Figure 4.18: Parallel RLC circuit match to the radiation impedance of the CMUT element. Dashed lines show the RLC circuit characteristic.................................... 50

Figure 4.19: Equivalent circuit representation of the CMUT element with N cell 51

Figure 4.20: Obtained equivalent circuit model of the CMUT element used in experiments. 51

Figure 4.21: Input impedance comparison between equivalent circuit and ANSYS results for the CMUT element consists of 16 cells. 52

Figure A.1: Illustration of sacrificial layer method **Error! Bookmark not defined.**

Figure A.2 : Illustration of wafer bonding method. Thermal oxidized silicon substrate and SOI wafer (A). thermal oxide and silicon etch respectively to form the cavity (B). Silicon wafer fusion bond (C). Ground etch back and remove the box (D). Metal deposition and patterning (E). Thin oxide or nidride deposition as passivation layer and patterning (F). Wire bond to electrodes (G)... **Error! Bookmark not defined.**

Figure A.3 : Bonding energy of typical bonded hydrophilic oxidized silicon wafers as a function of annealing temperature. Both short and long annealing cases are shown [16]. **Error! Bookmark not defined.**

LIST OF TABLES

Table 2.1 : Device Parameters 4
Table 3.1 : Material Properties of Model.. 17
Table 4.1 : Physical parameters of fabricated CMUT arrays 38
Table 4.2 : ANSYS model parameters.. 45

LIST OF ABBREVIATIONS

CMUT : Capacitive Micomachined Ultrasonic Transducer

FEM : Finite Element Model

3D : Three Dimensional

2D : Two Dimensional

CMOS : Complementary-symmetry/metal-oxide semiconductor

AC : Alternating Current

DC : Direct Current

IVUS : Intravascular Ultrasound Imaging

LTO : Low Temperature Oxide

BOE : Buffered Oxide Etch

SOI : Silicon On Insulator

CHAPTER 1

INTRODUCTION

Ultrasound is used in a wide variety of applications. Non-destructive evaluation (NDE), medical imaging, ranging are the most common application areas. In the history of acoustical devices, piezoelectric materials (e.g., barium titanate and lead zirconate titanate) have dominated the transducer technology. Capacitive micromachined ultrasonic transducers (CMUTs) have been developed as an attractive alternative to conventional piezoelectric transducers [1]. Even though the first fabricated CMUTs are as old as the early piezoelectric transducers, they have not been popular due to high electrical strengths, on the order of a million volts per centimeter, are required for the operation. The advances in microfabrication technology enable to build up the CMUTs which are operable with low electrical strengths and manifest CMUTs high performance as compared to piezoelectric transducers. Moreover, its compatibility with integrated circuit (IC) fabrication technology enables near electronics to be integrated with the transducer. In addition, other advantages like its larger bandwidth and, array configuration possibilities bring CMUTs one step further.

CMUT technology is not simply a cost effective solution to piezoelectric transducer technology. CMUTs are also promising for high frequency applications such as intravascular ultrasound imaging (IVUS) enabling miniature probes. Recently, medical imaging community has taken the lead in commercialization of CMUT technology [2]. CMUTs operating at frequencies as high as 60 MHz have been fabricated and tested successfully [3, 4].

Moreover, the development in microelectronics and digital signal processing technology enabled processing high amount of data from transducer arrays. New algorithms have been developed for reconstructing and analyzing data obtained from the transducers, especially in ultrasonic imaging [5]. Nevertheless, transducer quality (e.g., bandwidth, sensitivity, dynamic range) is the first limitation to activate and make these algorithms useful.

The increased interest in CMUT technology also increased the studies on the modeling. Fabrication of test samples requires several process steps and takes long time.

Accurately modeled transducer provides user to optimize the device parameters without fabrication. Depending on the target of the application a good design is very important to get the maximum efficiency from the transducer. Moreover, the overall system design can be upgraded with known transducer model.

The objective of the thesis to find an improved FEM which predicts the transducer behavior and can be optimized in a simulation environment to accommodate the conditions required for a target of application.

In Chapter 2, the theory of the device is given and first order model of the CMUT is introduced to describe the operation principle clearly. At the beginning of Chapter 3, FEM model is presented and the Mason equivalent circuit is introduced, the model is ensured by theoretical calculations. As a comparison with the experimental data, FEM model is constructed with the previously known parameters of fabricated CMUTs. Then the equivalent circuit of a single cell is presented. In Chapter 4, fabricated CMUT elements with different number of cells are characterized and hydrophone measurements are done. The measurement results are found to be precisely matching with FEM. Later, an accurate equivalent circuit model of the corresponding CMUT device is built and the results are presented. Lastly, conclusions and future work are given in Chapter 5. In the appendix A the fabrication method of CMUTs are introduced and the methods are compared.

CHAPTER 2

FUNDAMENTALS: CMUT

This chapter serves as an introduction to the Capacitive Micromachined Ultrasonic Transducer (CMUT). The first section describes the CMUT structure and operating principle.

The section is followed by first order model of CMUT to give insight of a single CMUT behaviour. In the next section, Mason equivalent circuit model is introduced and a theoretical expression of each parameter is given.

2.1 CMUT Structure

The basic CMUT structure is a capacitor consisting of a metalized membrane suspended above an electrically conductive substrate as shown in Figure 2.1.

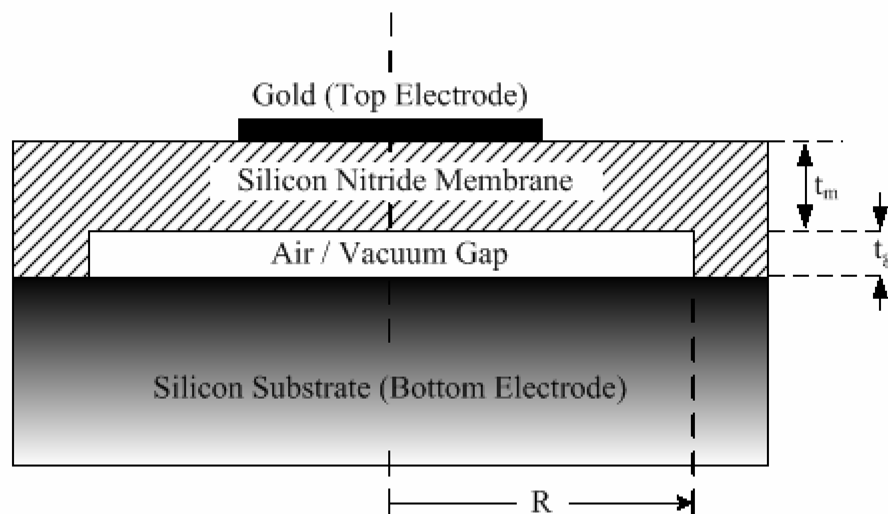

Figure 2.1 : Cross sectional view of a CMUT cell

The operating principle of the device is basically the vibration of the membrane by the electrostatic attraction force between the two electrodes. Generally, silicon substrate is used as bottom electrode in order to simplify the fabrication but it is also

shown that the patterned bottom electrode improves CMUT performance [6]. The device is axis symmetric around the dashed line shown in the center of the figure. Membrane material is silicon nitride and it is supported from posts by the same material. The post shows variety depending on the fabrication method. For immersion applications, a thin oxide layer is deposited on the overall structure to isolate top electrode. Typical CMUT parameters are given in Table 2.1.

Device Parameters	
Membrane thickness (t_m), μm	1
Gap thickness (t_g), μm	0.3
Membrane radius (R), μm	15
Top electrode thickness, μm	0.2
Top electrode radius, μm	7.5
Silicon substrate thickness, μm	500

Table 2.1 : Device Parameters

Figure 2.2 shows the visualization of a CMUT 2D array element formed by the combination of 25 CMUT cells. The transparent areas under the circular top electrodes are the cavities. Substrate is used as bottom electrode shown the in right side of the figure. The pad for the bottom electrode is formed by etching the layers on the substrate.

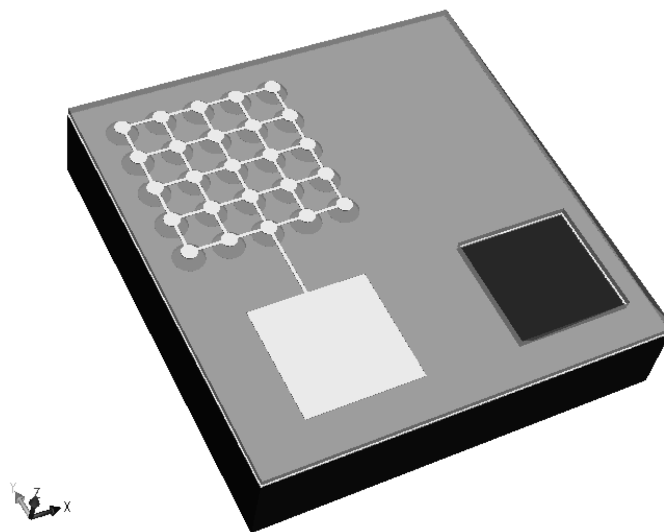

Figure 2.2 : 3D visualization of a CMUT 2D array element

2.2 Operating Principle

Most of the capacitive transducers operate by the variation of the distance between the electrodes as a function of time. When a static voltage is applied between the two electrodes, the membrane is forced to move towards the substrate by Coulomb forces. When an AC voltage is added to this DC voltage, the membrane starts to move simultaneously in response to that alternating signal and an ultrasonic wave is generated from this vibration and launched into the environment. Similarly, any incident ultrasonic wave vibrates the membrane and an AC signal is generated. DC voltage is also necessary in receiving operations because it supplies the required charge which is then modulated by the action of membrane to produce the AC signal. It is an important parameter which positively affects the devices efficiency. But there is a limitation on that DC voltage. After a certain level, which is named as the collapse voltage ($V_{collapse}$) , the membrane reaches the substrate and the device becomes unoperational.

2.3 First Order Model

The first order model of CMUT describes the operation behavior clearly [1]. To simplify the analysis some assumptions have to be done:

-Parallel plates

-Membrane restoring force is a linear function of displacement

-Neglecting all electrical fringing fields

-Perfect conductors

-Vacuum environment

After doing these assumptions, single CMUT element is presented by the lumped electromechanical model of Figure 2.3.

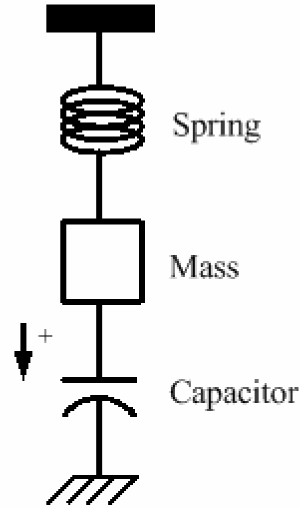

Figure 2.3 : Lumped first order model of a CMUT

In the figure, mass represents the mass of the membrane, capacitor stands for electrostatic force and spring models the restoring force of the membrane. The restoring force results from the resistance shown by the membrane residual stress. And d'Alembert's principle states that when we have a dynamic system the sum of all applied forces/moments should equal zero.

$$F_{spring} + F_{mass} + F_{capacitor} = 0 \tag{2.1}$$

Force on the capacitor is found writing capacitor equations:

$$C = \frac{\varepsilon A}{d_0 - x} \tag{2.2}$$

where C is the capacitance, ε is the permittivity, A is the plate area, d_0 is the static plate separation, x is the displacement in the direction shown in Figure 2.3.

$$\begin{aligned} E &= \frac{1}{2} C V^2 \\ &= \frac{1}{2} \frac{\varepsilon A}{d_0 - x} V^2 \end{aligned} \tag{2.3}$$

$$F = -\frac{dE}{dx}$$

$$= \frac{1}{2}V^2 \frac{\varepsilon A}{(d_0 - x)^2} \tag{2.4}$$

The force resulted by the mass is simply $F_{mass} = ma$, and the spring exerts a force which is linearly proportional to displacement,

$$F_{spring} = -kx$$

where k is the spring constant. Substituting these equations into (2.1) and writing the time dependencies

$$ma + \frac{1}{2}[V(t)]^2 \frac{\varepsilon A}{[d - x(t)]^2} - kx(t) = 0 \tag{2.5}$$

$$m\frac{d^2x(t)}{dt^2} + \frac{\varepsilon A[V(t)]^2}{2[d_0 - x(t)]^2} - kx(t) = 0 \tag{2.6}$$

Under static bias there is no time dependence, eliminating this terms leads to

$$\frac{\varepsilon A[V_{DC}]^2}{2[d_0 - x]^2} = kx \tag{2.7}$$

This equation has three real roots for small V_{DC} values but only one solution is stable where $x < d_0$. As mentioned before there is a limitation for V_{DC}. As bias voltage is increased, electrostatic forces added to gravitational forces exceed the restoring force and cause the membrane to collapse. This situation occurs when the displacement is one-third of the total gap distance. Solving the equation (2.7) for $x = d_0/3$,

$$V_{Collapse} = \sqrt{\frac{8kd_0^3}{27\varepsilon A}} \tag{2.8}$$

The increase in the bias voltage also causes a decrease in the spring constant. Since the electrode plates come closer to each other, the electrostatic force will be higher, moving the membranes much more. This increase in force is described as spring

softening [7]. It can be shown mathematically with Taylor expansion of electrostatic force about the point $x(t) = x^*$

$$m\frac{d^2x(t)}{dt^2} + \frac{\varepsilon A(V^*)^2}{2(d_0 - x^*)^2} + \frac{\varepsilon A(V^*)^2}{(d_0 - x^*)^3}\left[x(t) - x^*\right] - kx(t) = 0 \qquad (2.9)$$

Rearranging the equation in a similar form of the previous one,

$$m\frac{d^2x(t)}{dt^2} + \frac{\varepsilon A(V^*)^2}{2(d_0 - x^*)^2}\left[1 - \frac{2x^*}{(d_0 - x^*)}\right] - \underbrace{\left(k - \frac{\varepsilon A(V^*)^2}{(d_0 - x^*)^3}\right)}_{k_{soft}}x(t) = 0 \qquad (2.10)$$

where,

$$k_{soft} = k - \frac{\varepsilon A(V^*)^2}{(d_0 - x^*)^3} \qquad (2.11)$$

It can be easily seen that spring constant decreases with the increase of bias voltage applied to the membrane. First order model also give insight to small signal behaviour of CMUT. If we assume that the membrane displacement x is small compared to gap spacing d_0, electrostatic force will be

$$F_{capacitor} \approx \frac{1}{2}V^2\frac{\varepsilon A}{(d_0)^2}$$

where electrostatic force is proportional to square of applied voltage ($V = V_{DC} + V_{AC}$),

$$F_{capacitor} \propto V_{DC}{}^2 + 2V_{DC}V_{AC} + V_{AC}{}^2 .$$

A second assumption can be done by choosing $V_{DC} >> V_{AC}$, the time varying force will be

$$F_{capacitor} \propto 2V_{DC}V_{AC} .$$

These results can be easily seen experimentally which will be further discussed.

2.4 Electrical Equivalent Circuit Model

The basic method to examine the performance of the design is to use an electrical circuit model. The goal of this approximation is to explain the design criteria in electrical terms and to facilitate the design of transmitting and receiving circuits. The model can be easily tested with circuit simulators with its front-end circuits to check electrical bandwidth and insertion loss. Mason's equivalent circuit model is widely used for CMUT modelling. The electrical circuit model, shown in Figure 2.4, consists of two port network, where one side is in electrical domain and the other one is in mechanical. On mechanical side of the circuit, voltage represents force and current represents velocity. Input of the circuit is the source voltage with a resistive component R_s. Voltage is then converted to force, F, using a transformer with a transformer ratio n. Force is assumed to be uniform over the membrane and velocity, v, refers to average velocity of the membrane. C_0 is the device capacitance and Cp is the parasitic capacitance which will be described in the device parameters section. Z_{mem} is the mechanical impedance of the membrane and Z_{rad} is the radiation impedance of the surrounding medium. And there is shown a minus sign component $-C_0/n^2$ which plays the role of spring softening and it will be entitled as spring softening capacitor.

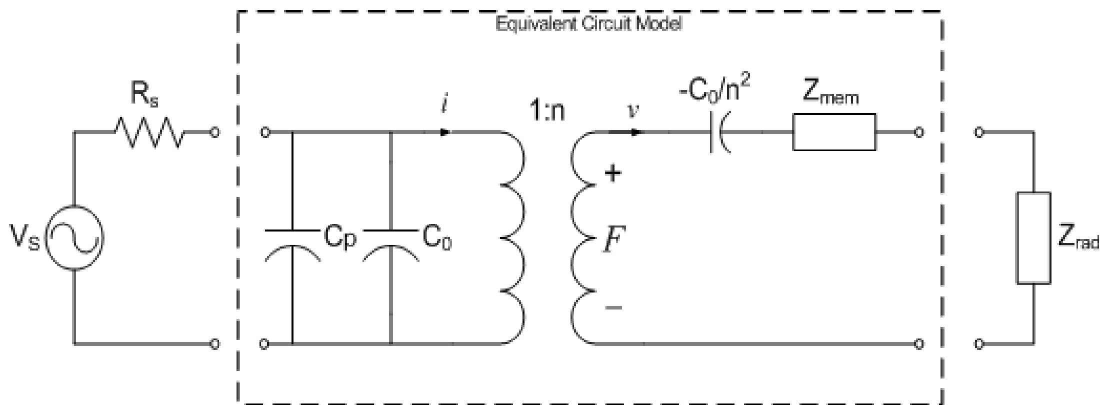

Figure 2.4 : Electrical equivalent circuit of a CMUT

2.4.1 Mechanical Impedance of the Membrane: Z_{mem}

According to Mason, membrane deflection under a constant pressure (P) is as

$$\frac{(Y_0+T)t_m^3}{12(1-\sigma^2)}\nabla^4 x(r) - t_m T\nabla^2 x(r) - P - t_m\rho\frac{d^2x(r)}{dt^2} = 0 \qquad (2.12)$$

where $x(r)$ is the normal displacement, t_m is the thickness, T is the residual stress, Y_0 is the Young's modulus, and σ is the Poisson's ratio, ρ is the density of the membrane. If we write the same equation for the case of harmonic excitation

$$\frac{(Y_0+T)t_m^3}{12(1-\sigma^2)}\nabla^4 x(r) - t_m T\nabla^2 x(r) - P - w^2 t_m\rho.x(r) = 0 \qquad (2.13)$$

where w is the angular frequency. As we know, the displacement at the edges of the membrane will be zero, $x(r)\big|_{r=R} = 0$, and its derivative at these points will also be zero $\left.\frac{dx(r)}{dr}\right|_{r=R} = 0$. Solving the eqn. (2.13) for these boundary conditions yields to

$$x(r) = \frac{P}{w^2\rho t_m}\left[\frac{k_2 J_0(k_1 r)J_1(k_2 R) + k_1 J_0(k_2 r)J_1(k_1 R)}{k_2 J_0(k_1 R)J_1(k_2 R) + k_1 J_1(k_1 R)J_0(k_2 R)} - 1\right] \qquad (2.14)$$

with

$$k_1 = \sqrt{\frac{\sqrt{d^2+4cw^2}-d}{2c}} \text{ and } k_2 = j\sqrt{\frac{\sqrt{d^2+4cw^2}+d}{2c}} \qquad (2.15)$$

where

$$c = \frac{(Y_0+T){t_m}^2}{12(1-\sigma^2)} \text{ and } d = \frac{T}{\rho} \qquad (2.16)$$

In eqn. (2.14) J_0 and J_1 are the Bessel functions of the first and second kind respectively. The velocity of the membrane can be calculated by taking the time derivative of the displacement, simply multiplying by jw,

$$v(r) = jwx(r)$$

the average velocity $\bar{v}$ is,

$$\bar{v} = \frac{1}{\pi R^2}\int_0^R\int_0^{2\pi} r.v(r).d\theta.dr$$

$$= \frac{jP}{w\rho t_m}\left[\frac{2(k_1^2 + k_2^2)J_1(k_1R)J_1(k_2R)}{Rk_1k_2\left(k_2J_0(k_1R)J_1(k_2R) + k_1J_1(k_1R)J_0(k_2R)\right)} - 1\right] \quad (2.17)$$

Membrane mechanical impedance is defined as the ratio of pressure to velocity. Finally, Z_{mem} can be written as,

$$Z_{mem} = jwPt_m\left[\frac{t_mRk_1k_2\left(k_2J_0(k_1R)J_1(k_2R) + t_mk_1J_1(k_1R)J_0(k_2R)\right)}{Rk_1k_2\left(k_2J_0(k_1R)J_1(k_2R) + k_1J_1(k_1R)J_0(k_2R)\right)} - 1\right] \quad (2.18)$$

Noting that we are in the mechanical domain, the force-velocity conventions are used, this parameter must be multiplied with the device area before replacing it into equivalent circuit model. Also, impedance of the membrane can be represented by a series LC circuit as shown in Figure 2.5.

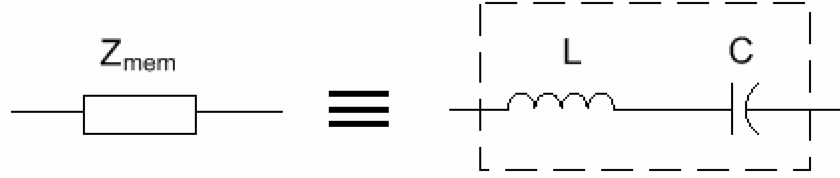

Figure 2.5 : Equivalent circuit representation of membrane impedance for the first harmonic excitation

2.4.2 Device Capacitance: C_0

The electrical capacitance of a CMUT cell with a membrane thickness of t_m and a gap of t_g can be written as:

$$C(t) = \frac{\varepsilon A}{t_m + \frac{\varepsilon}{\varepsilon_0} t_g(t)} \quad (2.19)$$

where ε_0 is the dielectric constant of air, and ε is the dielectric constant of the membrane material. It must be noted that this calculation is valid for full metal deposited membrane. It can be easily calculated using simulation tools for different electrode shapes. Optimization of the electrode radius has been done [8].

2.4.3 Transformer Ratio: n

Transformer ratio is a coefficient that represents the electrical parameters in mechanical domain. It can be obtained after some mathematical calculations starting with equation of current flow through the device:

$$I = \frac{d}{dt}Q = \frac{d}{dt}\left[C(t)V(t)\right] = C(t)\frac{d}{dt}V(t) + V(t)\frac{d}{dt}C(t) \tag{2.20}$$

Total voltage can be written in the form of

$$V = V_{DC} + V_{ac}\sin(wt)$$

where $V_{ac} << V_{DC}$ is the small signal AC voltage. Capacitance value can also be written in the same form

$$C(t) = C_0 + C_{ac}\sin(wt + \phi).$$

$C_{ac} << C_0$. If the equation (2.20) is rewritten

$$I = C_0\frac{d}{dt}V_{ac}(t) + V_{DC}\frac{d}{dt}C_{ac}(t) \tag{2.21}$$

substituting C_0 into the equation and taking the derivative,

$$\frac{d}{dt}C_{ac}(t) = -\frac{\varepsilon_0\varepsilon^2 A}{(\varepsilon_0 t_m + \varepsilon t_{g0})^2}\frac{d}{dt}t_g(t) \tag{2.22}$$

where t_{g0} is the DC value of the gap spacing. The derivative of the air gap distance represents the membrane velocity

$$\frac{d}{dt}t_g = \bar{v}$$

rewriting the eqn. (2.21) with velocity parameter leads to

$$I = C_0\frac{d}{dt}V_{ac}(t) - V_{DC}\frac{\varepsilon_0\varepsilon^2 A}{(\varepsilon_0 t_m + \varepsilon t_{g0})^2}\bar{v} \tag{2.23}$$

This equation shows the relation of the two different parameters (current and velocity) which are in different domains. If the current is written in that form

$$I = C_0 \frac{d}{dt} V_{ac}(t) - n\bar{v}$$

Transformer ratio can be defined as

$$n = V_{DC} \frac{\varepsilon_0 \varepsilon^2 A}{(\varepsilon_0 t_m + \varepsilon t_{g0})^2} \tag{2.24}$$

for small deflections transformer ratio is

$$n = V_{DC} \frac{C_0}{(t_m + \frac{\varepsilon}{\varepsilon_0} t_{g0})} = C_0 E \tag{2.25}$$

where E is the induced electric field. This equation state that turns ratio is equal to the product of the device capacitance and the electric field in the device. As seen from the above equations transformer ratio is changed with bias voltage, membrane shape and thickness.

2.4.4 Spring Softening Capacitor: $-C_0/n^2$

As previously described, a physical phenomenon, it is the change in spring constant caused by bias voltage. The change can be clearly understood looking into first order lumped model of CMUT. Due to bias voltage the membrane gets closer to substrate and the effect of electrostatic force increases. In that case any change in that force causes membrane to deflect much more. Deflection can be explained by the softening the spring constant, so this situation is defined as spring softening. From the first order model, spring softening was found with equation

(2.11), corresponding capacitor value is

$$C_{soft} = -\frac{(d_0 - x)^3}{\varepsilon A (V_{DC})^2} = -\frac{(d_0 - x)^2}{C_0 {V_{DC}}^2} = -\frac{1}{C_0 E^2} = -\frac{C_0}{n^2}$$

This parameter should be included in the final equivalent circuit in order to make the model to be more factual.

2.4.5 Parasitic Capacitor: C_p

Parasitic capacitance is an important parameter which highly affects the transducer efficiency. Especially when it exceeds the value of the device capacitance, it would be impossible to use CMUT in receive mode where capacitance change is so important. There would be two different source of the parasitic capacitance [6]. The first source of the parasitic capacitance is the overlapped area between bond pads and the bottom electrode where it can overwhelm the active capacitance of the device. The solution of the problem is to pattern the bottom electrode instead of using a conductive substrate. And the second source of parasitic capacitance is caused by electrical interconnects and amplifier circuits. In that case a careful design of the amplifier circuit is required.

2.4.6 Radiation Impedance of the membrane: Z_{rad}

Due to the motion of the membrane, the surrounding acoustic medium exerts a reaction force on it with respect to the velocity of the membrane. This resistance is called the radiation impedance. The calculation of this impedance is a complex issue. The derivations have been done for a plane piston radiator. As the same movement is done by CMUT, radiation impedances will have same characteristic. Normally, radiation impedance equals to the acoustic impedance of radiating medium Z_{medium} multiplied by the transducer area A. Radiation impedance can be expressed as

$$Z_r = A.Z_{medium} = A(R_r + X_r)$$

where R_r is the radiation resistance and X_r is the radiation reactance. When the transducer radius R is greater than operating wavelength λ then the reactance of the radiation impedance goes to zero and only the reactive part manifest itself. But when the transducer radius is smaller than the wavelength then this reactive part should be included in the equivalent circuit representation. Moreover, anti-resonance occurs by the interactions between cells which limit the overall bandwidth of the device. To include all that effects in the circuit radiation impedance is modeled by using FEM.

CHAPTER 3

FINITE ELEMENT MODEL

Equivalent circuit model simplifies most of the analysis but it is constructed on some basic assumptions (piston model movement, parallel plates, etc.). Finite element model gives more accurate result in order to model the CMUT and the overall array. The ANSYS software package is used for the finite element model. The theoretical tools employed in the simulations are presented and the CMUT model is introduced. Simulation results obtained by static, modal, harmonic and transient analysis are presented then compared to theoretical results described in chapter 2. The theoretical results are calculated in MATLAB. ANSYS results are also plotted in the same environment.

3.1 ANSYS Model

The finite element model is built using ANSYS 6.1 FEM Package. ANSYS enables acoustic analysis to solve acoustic wave propagation in a fluid medium. The ability to model the interaction between fluid and structural physics in ANSYS allows us to design a CMUT structure operating in fluid environment, in addition, optimizing device parameters with checking performance in an easy way without fabrication.

Modelling is the fundamental step to get precise results. In order to see CMUT array behaviour, 3D model is used. Modelling starts with a membrane. SOLID45 elements are suitable for membrane modelling. The element has plasticity, creep, swelling, stress stiffening, large deflection, and large strain capabilities which are enough to model the membrane. FLUID30 elements are used to model immersion medium. The fluid-structure interface is specified using proper fluid-structure interaction flags. Absorbing boundary element FLUID130 is used to extend the fluid domain to infinity. This element realizes a second-order absorbing boundary condition so that an outgoing pressure wave reaching the boundary of the model is “absorbed” with minimal reflections back into the fluid domain. Electrodes of the device are

modelled using TRANS126 electromechanical transducer elements. Single cell structure is shown in Figure 3.1.

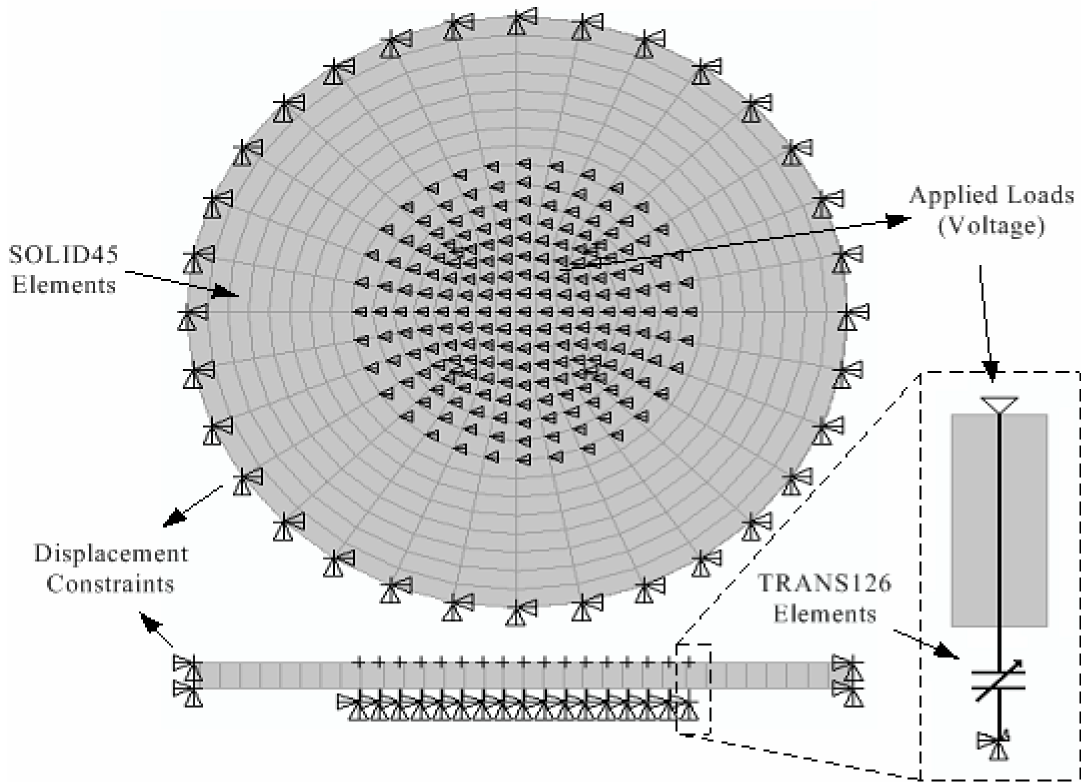

Figure 3.1 : 3D CMUT model with ANSYS elements

As membrane is fixed from the outer boundary, the exterior areas are not modelled. Displacement constraints at these points are set to zero. The gap under the cavity is vacuum, so there is no need to use a specific element to model the gap. Top electrode is formed by taking the surface nodes of the membranes. The top electrode is significantly smaller in thickness compared to the membrane material. Also the gold stiffness is much smaller than that of silicon nitride. Hence, the electrode is not included in the model for simplification. The electrode's position and driving force is defined by applying TRANS126 elements to relevant surface nodes of the membrane. As previously described, for a high efficiency operation electrode radius is found to be half of the membrane radius, so this structure is used throughout all analysis. Since surface nodes of the membrane are used as top electrode, substrate is formed by lower nodes of TRANS126 elements that are joined to upper surface nodes. Mechanical and

electrostatic properties of membrane material are entered as SOLID45 elements input, given in Table 3.1.

Membrane (Material)	Silicon Nitride
Young's Modulus (Pa)	3.20E+11
Density (kg/m^3)	3270
Poisson's Ratio	0.263
Dielectric Constant	7.6
Thermal Expansion Coefficient ($x10^{-6}$ K^{-1})	3.3

Table 3.1 : Material Properties of Model

In addition the number of mesh sizes is adjusted to have a high accuracy. The residual stress is an important drawback which highly affects the transducer resonant frequency, collapse voltage and, initial gap distance, it should be included in the finite element model. Basically, the stress occurs during deposition of the membrane material [9]. The stress could be applied to the membrane through the use of thermal properties of the SOLID45 element. In order to do this membrane edges are properly constrained and a thermal stress is introduced. The peak thermal stress generated at the surface when the material is subjected to an infinite heat transfer rate is determined by the following formula;

$$\sigma_{stress} = \frac{-E\alpha\Delta T}{1-v} \tag{3.1}$$

where σ_{stress} is thermal stress, E is the young modulus, α is the thermal expansion coefficient of the membrane material, v is the poisson ratio and

$$\Delta T = T - T_{ref}$$

is the temperature change with respect to reference temperature . When reference temperature is set to zero, required temperature change for a given stress value is.

$$T = \frac{-\sigma_{stress}(1-v)}{E\alpha} \tag{3.2}$$

Corresponding residual stress can be determined using temperature change. Typical value of 124.5MPa is assumed to be induced in the membrane. Figure 3.2, illustrates the stress distribution induced in the silicon nitride membrane with thickness of 1 micron, colour bars represents the stress in MPa.

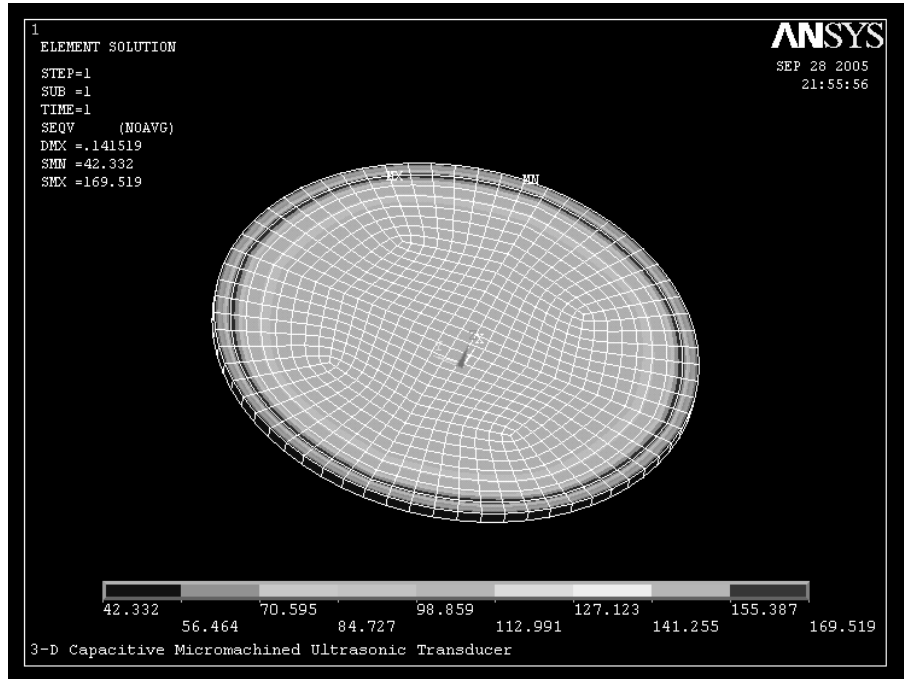

Figure 3.2 : Residual stress induced in membrane (MPa)

3.2 Static Analysis

This stage forms the basis of the harmonic analysis. The shape and the capacitance of the device for an applied bias can be found by static analysis. The collapse voltage information can also be extracted with that analysis. The result of the static analysis is taken as an input to harmonic analysis. Before starting static analysis, device capacitance is calculated using ANSYS “cmatrix” macro. This macro takes the input of electrode node components and calculates the self and mutual capacitances between them. A capacitance deflection curve obtained using a series of static analysis and remorphing the shape in each step. By this way the capacitance values for each deflected membrane position is calculated and stored (Figure 3.4). The stored data can be directly given to input of TRANS126 elements to get a realistic simulation results. Prestress effects are turned on to include residual stress of the membrane. Collapse voltage of the CMUT is found by doing some iteration, increasing the applied voltage is increased in each step, and solution convergence is checked. Static solution checks the status of the membrane deflection depending on the gap distance. When the deflection reaches one third of the gap distance solution does not converge. So, previous point before the unconverged static solution is taken as the collapse voltage. Input capacitance

under a DC bias can be obtained reading the capacitance output of the TRANS126 elements after the static analysis.

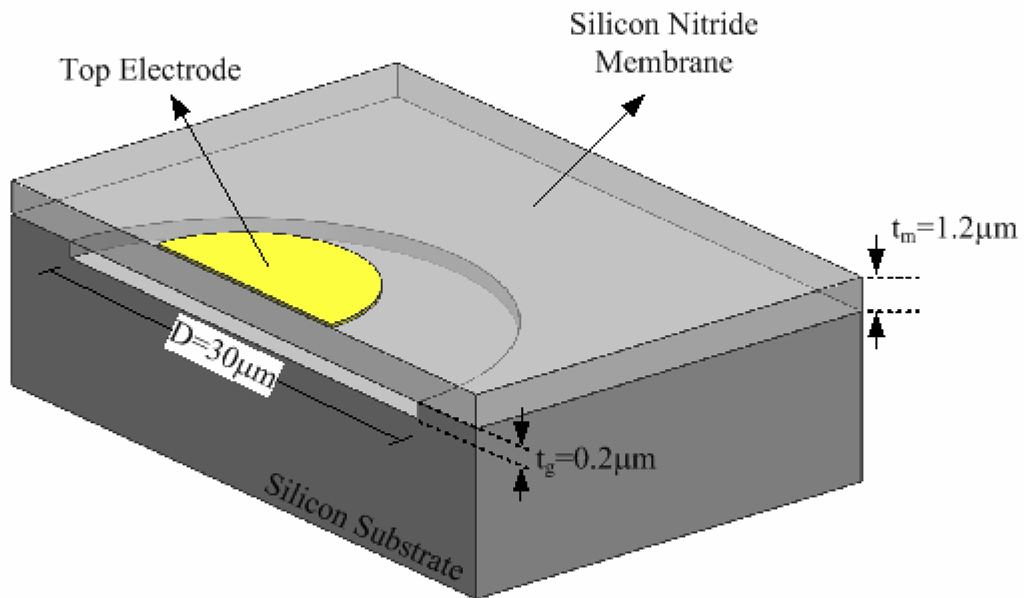

Figure 3.3 : The device geometry used in the analysis

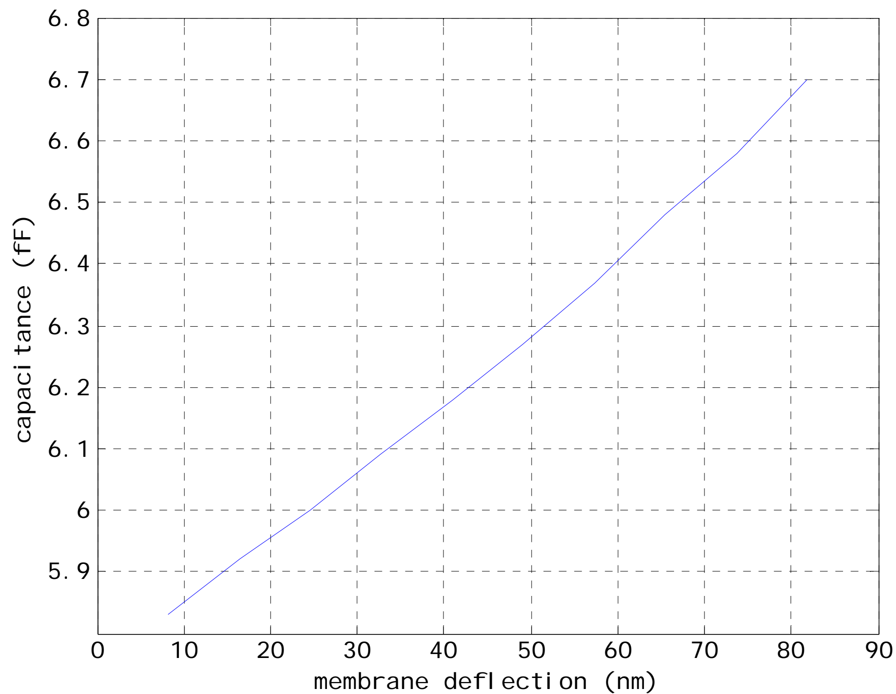

Figure 3.4 : Capacitance vs. deflection curve of the membrane in Figure 3.3. (Note that these values are calculated as half electrode)

The capacitance curve shown in Figure 3.4 is used for calculation of collapse voltage. Collapse voltage for the top electrode with half coverage of the membrane is

found as 161V. For the rest of the simulations membrane DC bias is simply set to 80% of the collapse voltage which is 128V.

3.3 Modal Analysis

Modal analysis determines the resonant frequency and mode shapes of the membrane. Before doing a harmonic analysis, resonant frequencies are extracted and then a harmonic analysis is done around first resonant frequency. Figure 3.5 illustrates the first mode shapes of the membrane.

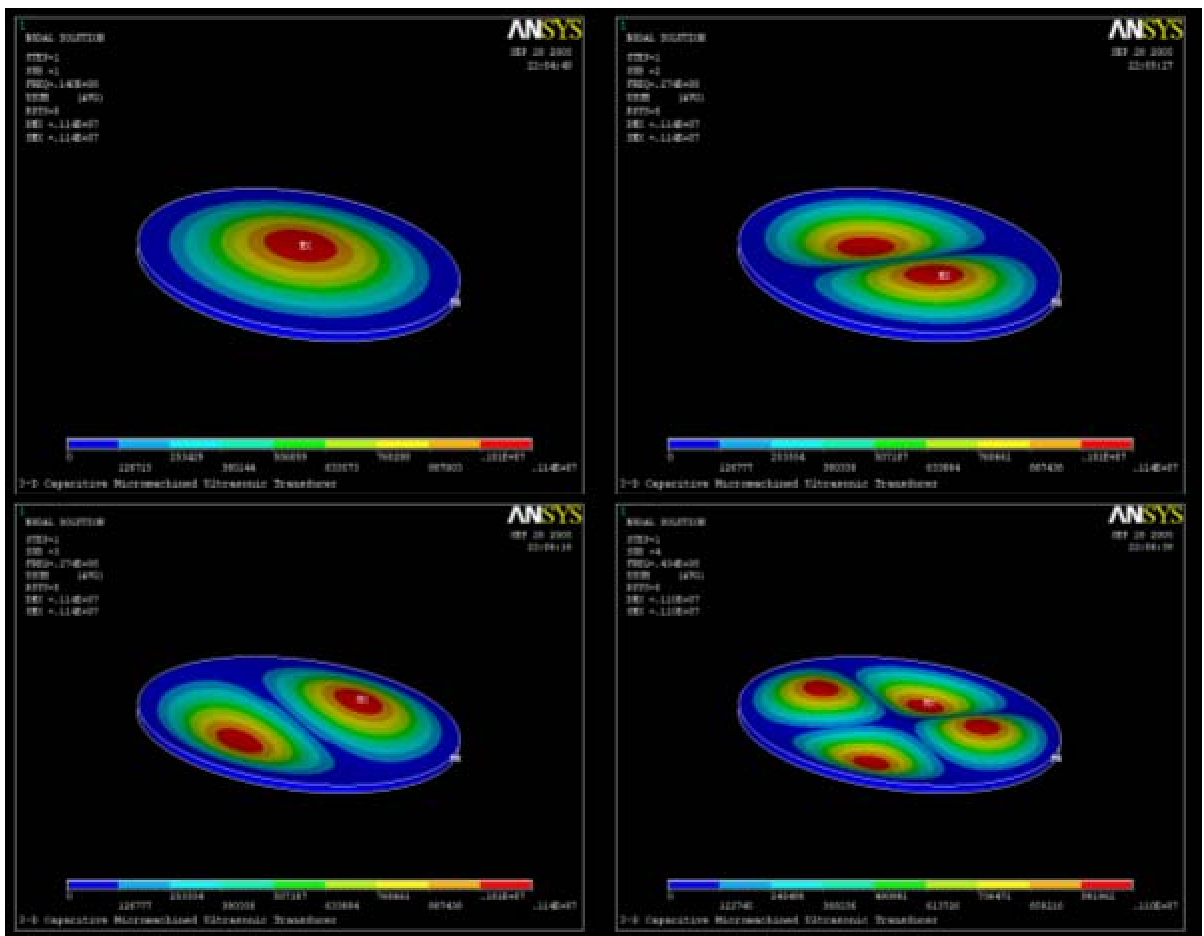

Figure 3.5 : Cmut operating modes. Fundemental mode (Top left). Second mode (Top right). Third mode (Bottom left). Fourth Mode (Bottom right).

3.4 Harmonic Analysis

A harmonic analysis, by definition, assumes that any applied load varies harmonically (sinusoidally) with time. In that case harmonic analysis provides the load that plays the role of AC voltage. While electromechanical elements are used in the structure, harmonic analyses require a static analysis done previously. By taking deflected membrane shape as a base that results from the static analysis, harmonic analysis is run. As a result, surface pressure, velocity distribution, and electrostatic force values and, etc. can be extracted with a frequency dependency. Moreover, input and acoustic impedance of the membrane, radiation impedance, and bandwidth of the structure can be calculated. The results are presented using the model in Figure 3.3.

Figure 3.6 shows prestressed harmonic analyses done over different static analyses. Maximum displacement is achieved at the resonant frequency. As a result of spring softening membrane series resonant frequency shifts down with increased bias voltage.

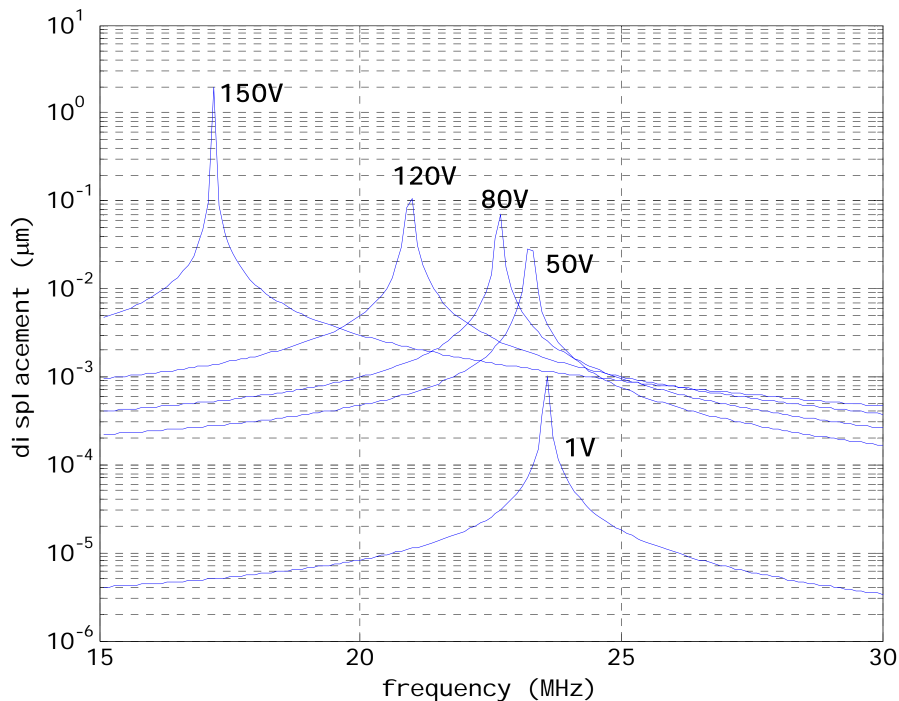

Figure 3.6 : Average displacement over the membrane

3.5 Membrane Mechanical Impedance

The mechanical impedance is the ratio of applied force to resulting velocity. To calculate membrane impedance Z_{mem} fluid medium is not modelled to eliminate the load over the membrane. If we turn back to Mason model when membrane is operating in vacuum the circuit output is shorted. By doing harmonic analysis the effective force over the membrane and average surface velocity in the frequency range of interest can be calculated. Membrane impedance can be calculated using the formula,

$$F_{effective}(w) = \bar{v}(w) Z_{mem}(w)$$

where effective force ($F_{effective}$) is, by mean, the force which is applied over the surface uniformly. When the half electrode constructed with TRANS126 elements, the total force will only be in the inner half radius area of the membrane. So to find the membrane mechanical impedance following method is used: firstly, a pressure value is applied over the membrane surface and a harmonic analysis is done, corresponding average velocity of the membrane is found. Secondly, the applied pressure is multiplied by the surface area to get $F_{effective}$ value and divided to the average velocity to find the membrane's mechanical impedance Z_{mem}. Figure 3.7 shows the imaginary part of the membranes impedance versus frequency. Real part of the impedance is zero because no loss parameter is included for membrane in the analysis.

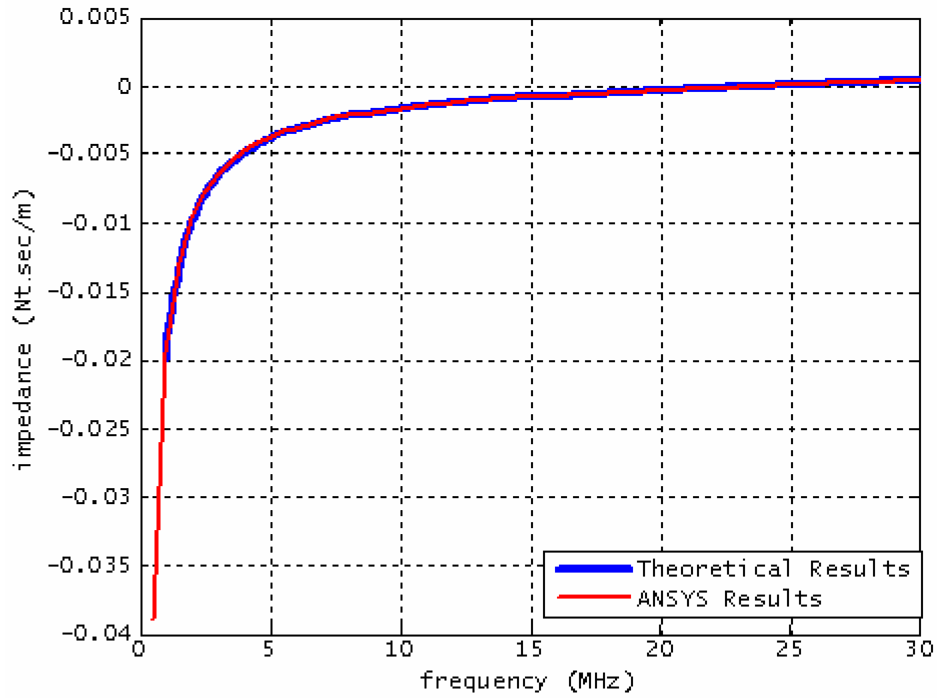

Figure 3.7 : Membrane impedance (R=15µm, t_m=1.2, t_g=0.2). Ansys results fit the theoretical results.

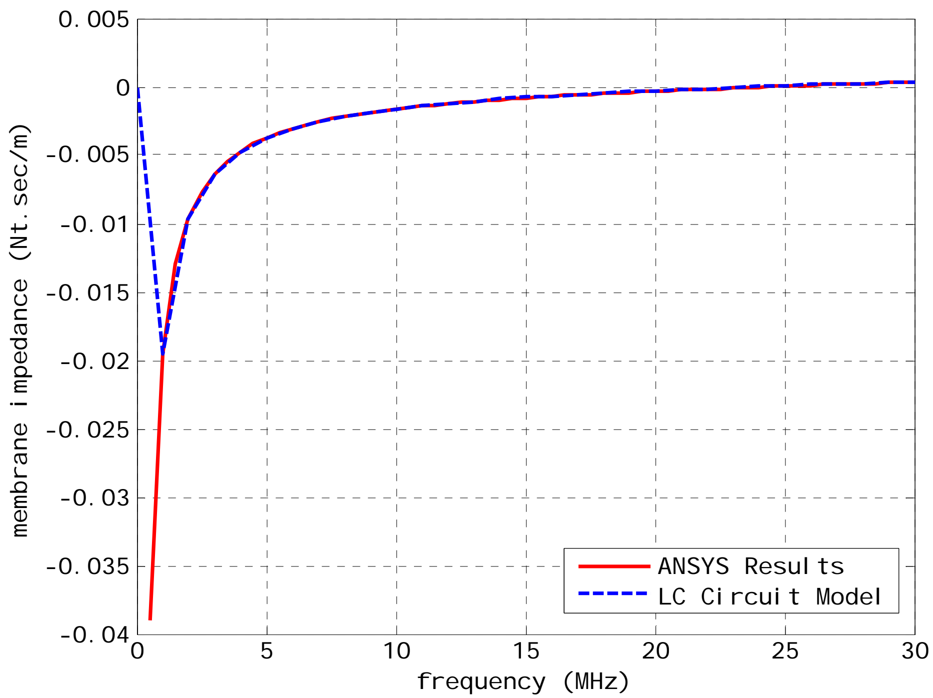

Figure 3.8 : Membrane impedance. LC circuit models the membrane impedance with a high accuracy where L=5.19pH and C=8.17µF

Membrane acoustic impedance is obtained with an LC circuit. The parameters are found with curve fitting method using MATLAB. As seen from the above figure membrane resonance occurs at the frequency of 24 MHz. Below that frequency imaginary part is negative that corresponds to the effect of conductor C in the circuit. Above the resonance frequency inductor effect is seen at the impedance curve. In a different way of point, capacitance refers to stiffness or spring constant and inductor refers to membrane mass in the model. In lower frequencies membrane mass is inactive but stiffness effect manifests itself and in higher frequencies the situation is vice versa.

3.6 Transformer Ratio: n

The transformer ratio is found with following equation [10],

$$n = \sum C_i E_i \tag{3.3}$$

where C_i and E_i are the capacitance and the electric field in each TRANS126 elements, respectively. After a static analysis for a given bias voltage, these parameters can be easily extracted by TRANS126 element's output definitions [11].

After finding the membrane impedance it becomes easier to find out the transformer ratio which is obtained dividing the effective force on the membrane to the applied AC voltage V_{AC},

$$n = \frac{F_{effective}(w)}{V_{AC}} = \frac{\bar{v} Z_{mem}}{V_{AC}}. \tag{3.4}$$

As is seen, transformer ratio is frequency dependent and makes small changes around resonant frequency especially when a high bias voltage is used. Mason model assumes the membrane with low deflection profile, so this change is omitted. Transformer ratio is plotted versus membrane thickness in Figure 3.9.

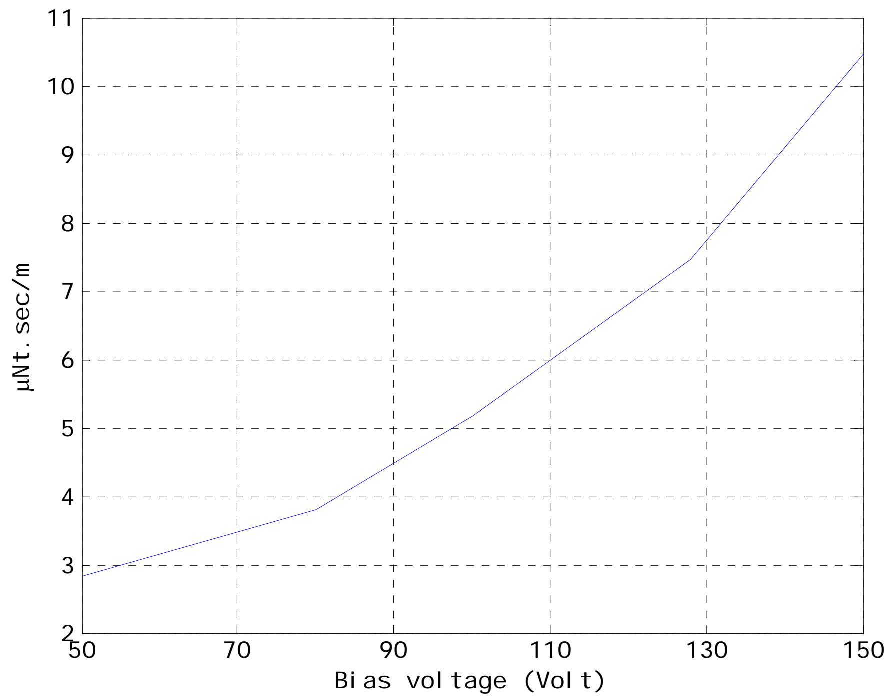

Figure 3.9 : Transformer ratio versus bias voltage.

It is found that transformer ratio for the device geometry shown in Figure 3.3 is equal to $7.45x10^{-6}$ Nt/V at 128V DC bias which is the 80% of the collapse voltage. Now, the circuit representation of a single CMUT element can be constructed, Figure 3.10. For air coupled operation the output of the circuit is shorted due to the mechanical impedance of the membrane is so larger than the radiation impedance of air. Input impedance of the following circuit is plotted in both case of air and water environment operation. No loss factor is introduced to membrane so there is no resistive component in the mechanical model and input impedance has only an imaginary part (Figure 3.11).

The behaviour of the input impedance can be explained with open and short circuit resonance terminology. Short circuit resonance occurs when the impedance of the right branch of the equivalent the circuit is zero where the source is shorted.

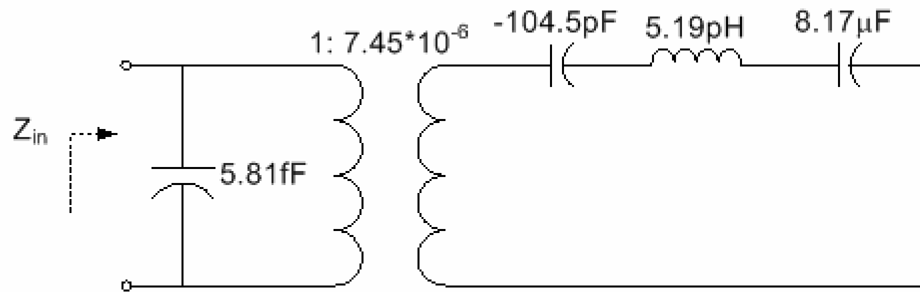

Figure 3.10 : Equivalent circuit model of a single air coupled CMUT

The open circuit resonance occurs when the membrane mechanical impedance is zero. In that case device capacitance becomes parallel to the spring softening capacitance. Their values will be same when the capacitance value in the mechanical domain is converted into the electrical domain, so they will cancel each other.

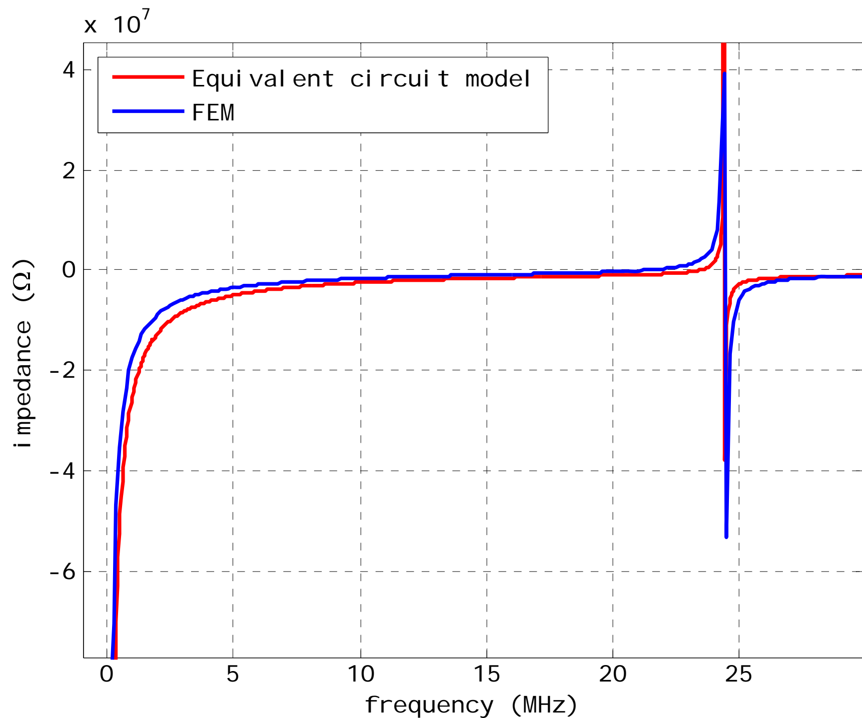

Figure 3.11 : Input Impedance comparison between equivalent circuit model and FEM for membrane geometry in Figure 3.3.

The input impedance obtained from Mason equivalent circuit and ANSYS results are compared. It found that transformer ratio calculated in the Mason model have to be corrected. The reason is the electrical forces are only applied to the electrode region in ANSYS model. But to find this value for the Mason model a uniform applied

force over the whole membrane is divided by the average velocity. For this correction an effective $n*$ for the given geometry can be defined which is in our model,

$$n* = 1.61n \tag{3.5}$$

If this effective transformer ratio value is used in the equivalent circuit model, a very good match between the circuit model and FEM model is obtained as shown in Figure 3.12.

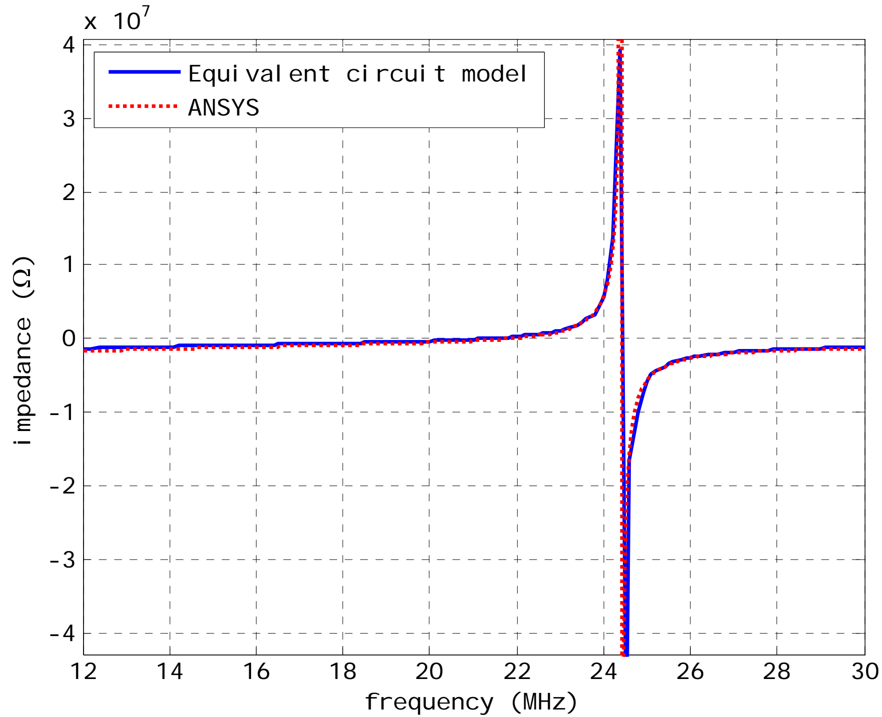

Figure 3.12 : Input impedance using improved circuit model and FEM

3.7 Immersed Operation

Up to here, mason model parameters are found, except radiation impedance that changes with radiating medium. In order to find the radiation impedance FLUID30 elements are used to model the fluid above the membrane. And it is extended with FLUID130 absorbing elements to infinite, by this means, immersed cMUT operation is settled. Sound velocity of 1480 m/sec. and density of 1000 g/m^3 is given as input parameter to fluid elements. When the fluid is included in the model it takes long times to complete the harmonic analyses, hence number of nodes highly increased. Mesh sizes are optimized to reduce the computation time, considering the accuracy carefully. Also

membrane is formed with displacement constraints as shown in Figure 3.13. For the immersion operation, target resonant frequency is chosen to be 10 MHz. Resonant frequency changes with radius and thickness parameters as described in chapter 1. Fabrication process limits the membrane thickness due to stress occurred in the membrane. It could be possible to increase resonant frequency with decreasing radius but 15µm radius is also quite small to do a good fabrication with conventional method. In addition when radius of the membrane decreases, electrode radius also decreases and it would be a problem in the receive mode operation where the effective capacitance would be less than the parasitic capacitance. So membrane thickness is increased to 1.2µm and the other parameters are not changed.

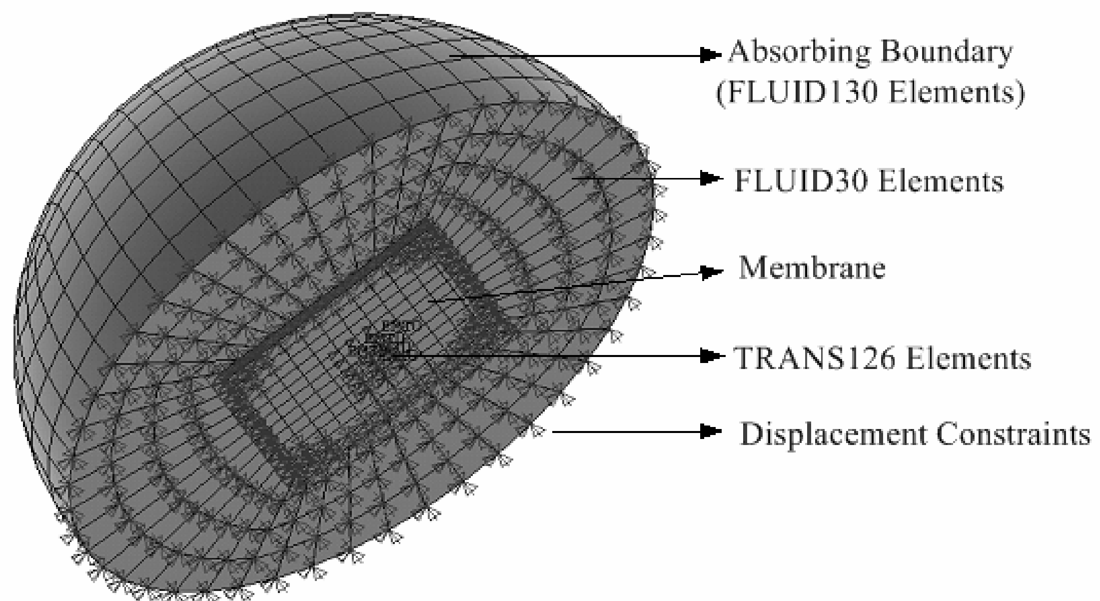

Figure 3.13 : Meshed model of immersed CMUT

It is found that operating frequency extremely decreases under fluid load. Displacement of the membrane is plotted for the same membrane in air and water environment. The applied DC voltage is fixed to 80% of the collapse voltage for efficient operation. Average pressure over the surface of the membrane is plotted in Figure 3.15. Single cell has around half of fractional bandwidth. It is also found that transient analysis give more accurate results in compare to harmonic analysis after the characterization of fabricated CMUTs where the results are given in chapter 5. It is found that harmonic analysis losses its efficiency at higher frequencies. This is due to

absorbing boundary. Absorbing boundary should be replaced to a distance of one wavelength from the vibrating surface. This is required for the absorbing element to work well to eliminate reflecting waves from the boundary. For that reason, the position of the absorbing boundary should be changed and the whole structure should also be remeshed in each frequency step but it increases the time required for the simulations which are already takes too much time.

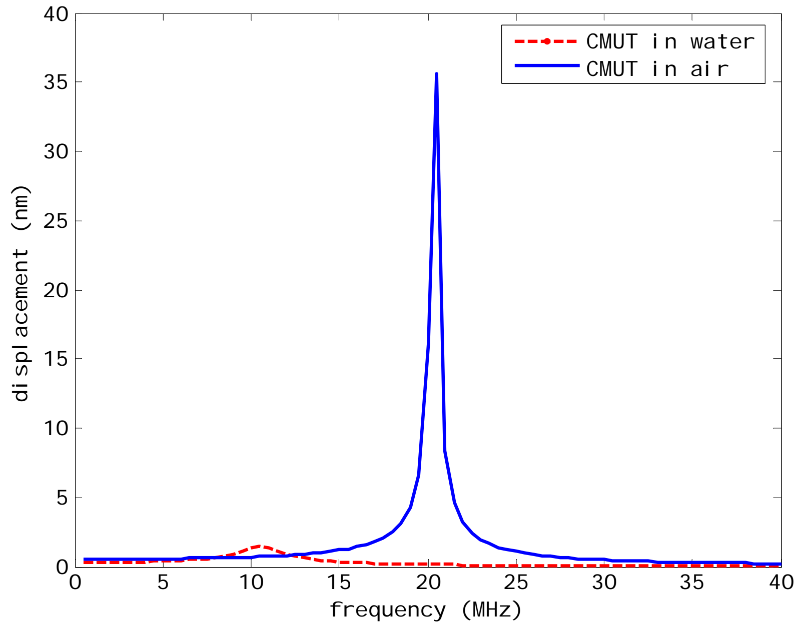

Figure 3.14 : Average displacement of the membrane in two different environments

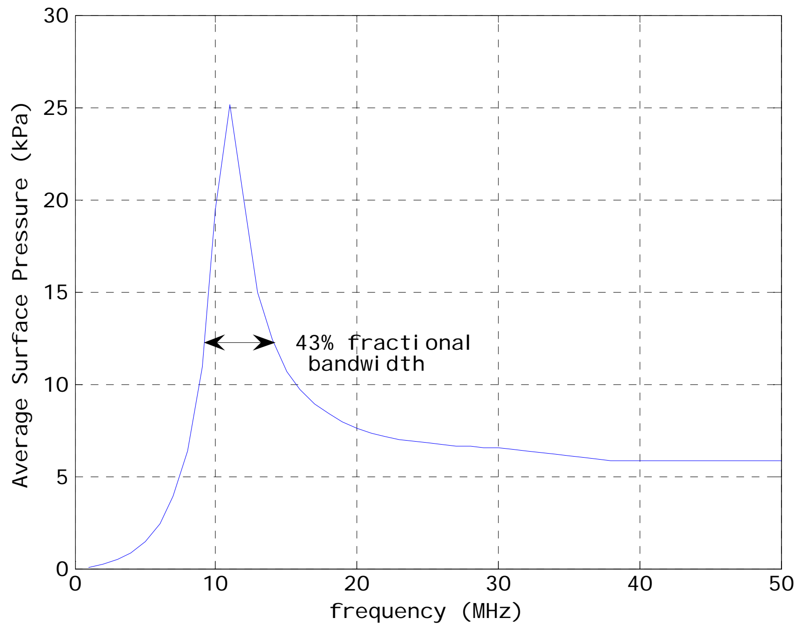

Figure 3.15 : Single cell surface pressure in water at a resonant frequency of 11 MHz

A comparison between harmonic and transient is done for surface average pressure measurement is shown in Figure 3.16.

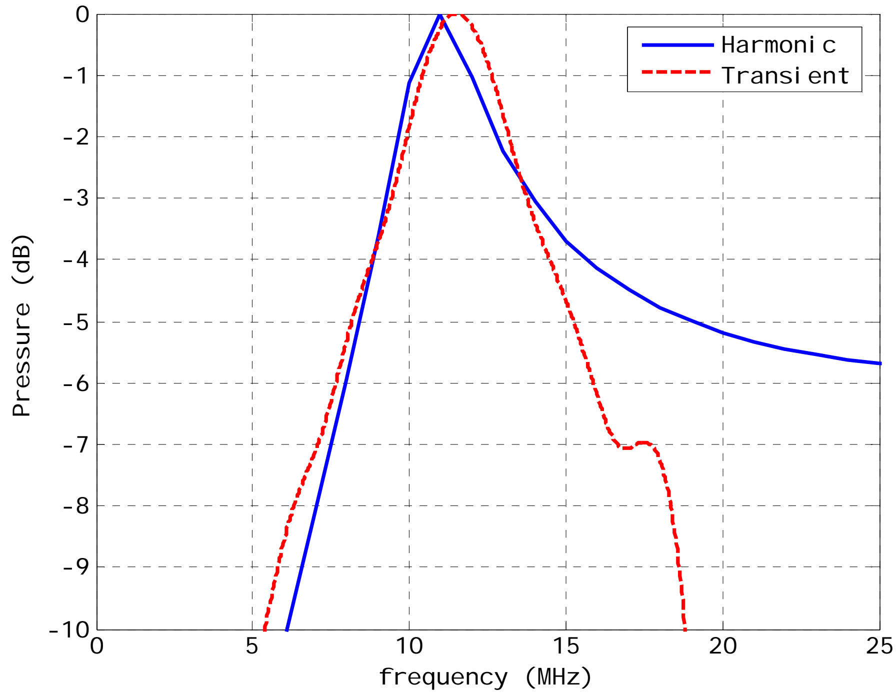

Figure 3.16 : Surface average pressure (harmonic and transient analysis comparison)

Radiation impedance is calculated by taking and averaging the surface integral of the pressure and then dividing this value to average membrane velocity. The real and imaginary part of the radiation impedance of a single cell is found as in Figure 3.17. The radiation impedance characteristic is similar as a piston radiator. It is shown that radiation impedance can be modeled with a parallel RLC circuit (Figure 3.18). The circuit models the radiation impedance with a good accuracy around the resonant frequency. Replacing previously found parameters, yields the circuit as shown in Figure 3.19.

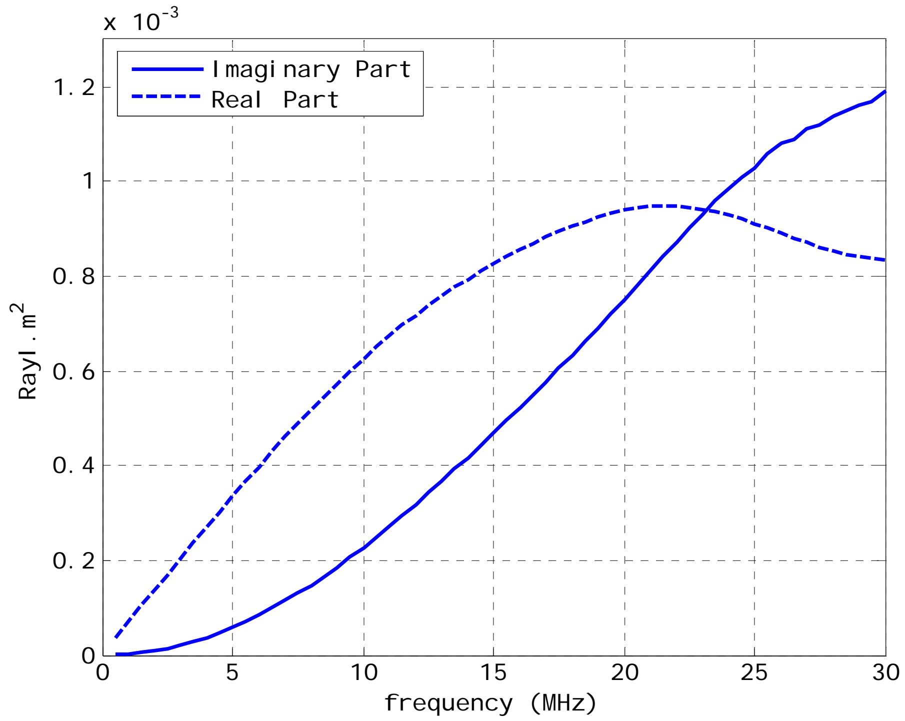

Figure 3.17 : Radiation impedance of a single CMUT cell

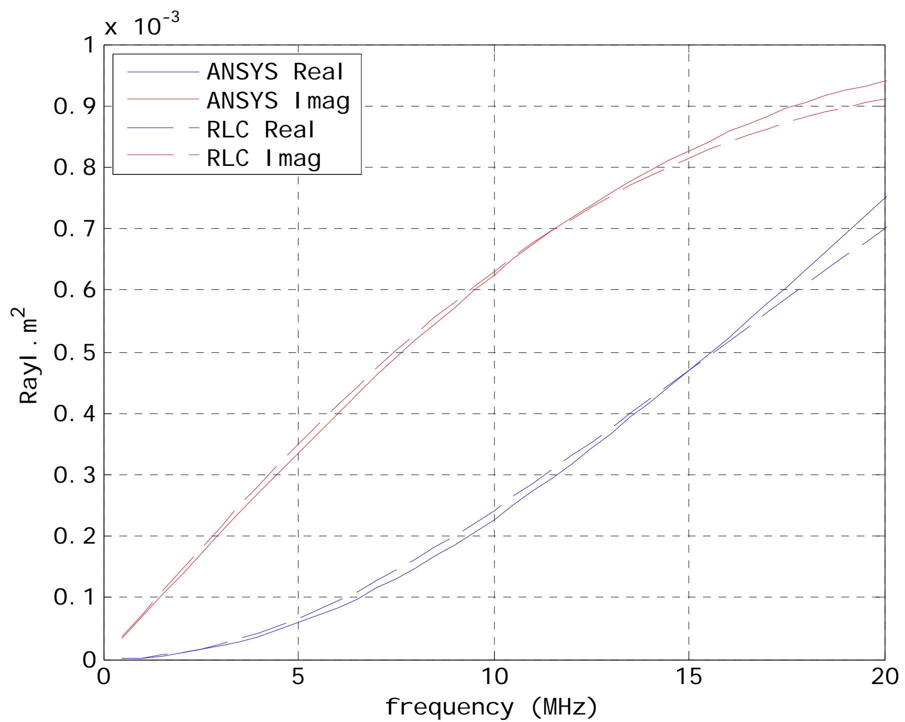

Figure 3.18 : Parallel RLC circuit model optimized for the radiation impedance found using MATLAB

(R=15.2μΩ, L=71fH,C=5.7pF)

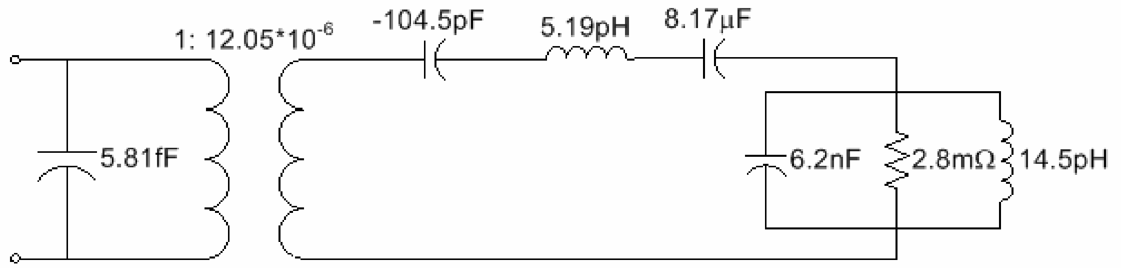

Figure 3.19 : Equivalent circuit model of a single immersion CMUT

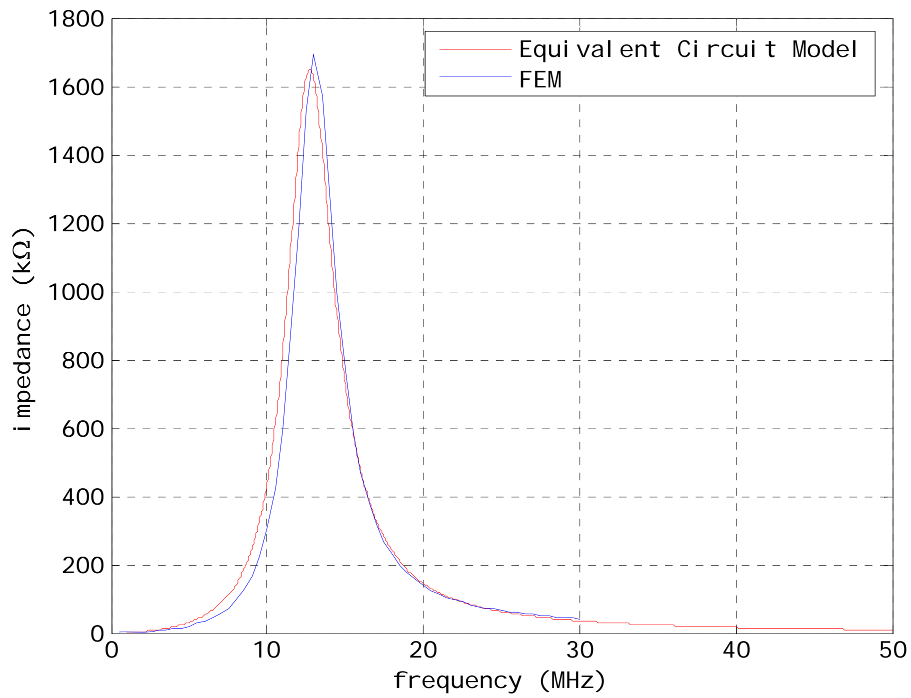

Figure 3.20 : Real part of input impedance of circuit shown in Figure 3.19.

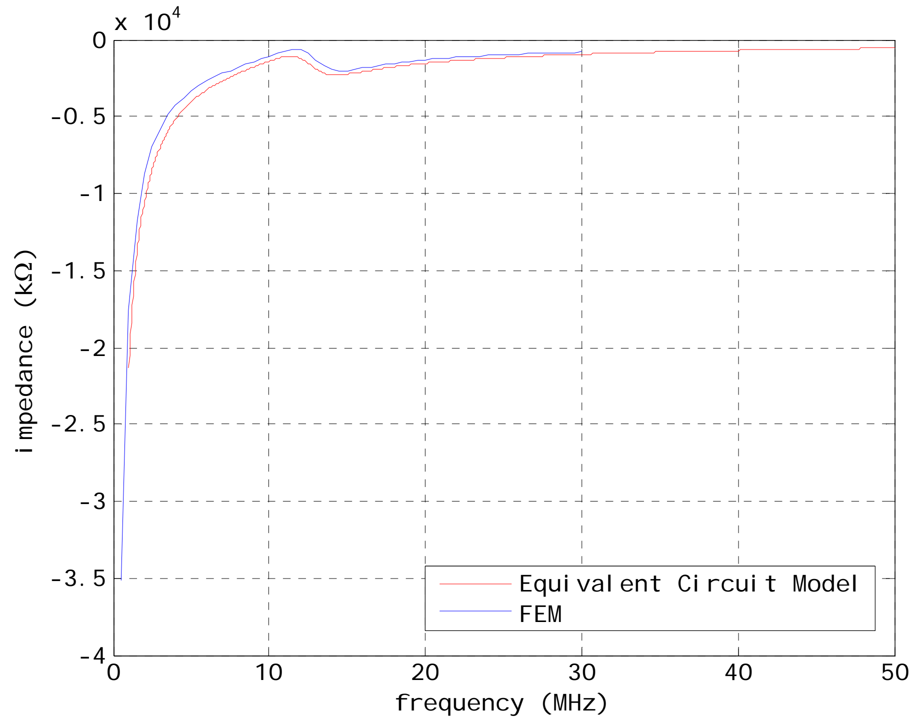

Figure 3.21 : Imaginary part of input impedance of circuit shown in Figure 3.19.

3.8 Transient Analysis

Transient analysis is used to determine the dynamic response of a structure under time-dependent loads. As a result, loads can be extracted on a time scale. It gives better insight to device operation. The results are more accurate rather than harmonic analysis, eliminating the absorbing boundary problem. In transient analysis, the time can be set in such a way that the analysis is finished before acoustic wave reaches the absorbing boundary or absorbing boundary itself is set to a far distance from the wave source. This provides no reflected waves from the boundary. In addition, time scaled parameters can be converted into frequency domain with Fourier transform. As TRANS126 elements are used in the model, device operation can be directly simulated in time scale. In that way, electrical port excitation is provided and the output is observed in terms of displacement, pressure, etc. It is also seen that transient analysis takes less time compared to harmonic analysis for the same device without changing number of elements or nodes.

Transient analysis is an individual analysis, so it does not require static analysis done before its run but it requires initial conditions to be given as input. If there is a nonzero initial condition like, in our case, a prestressed membrane with DC bias, the initial condition is set by performing a static analysis time-load step. For that purpose, a predefined DC voltage is applied to TRANS126 elements and the time integration effects are turned off in the first step. The length of the time for the first step is set to a small unessential value. The results taken from the first step is used as an initial condition for the subsequent load steps, so the applied bias voltage is included in all subsequent load steps for a true analysis.

This analysis is used to simulate the array operation in the work.

3.9 Array Operation

Previously described parameters are all to model a single CMUT behaviour. CMUT cells are usually combined to form array elements used in phased array imaging. When cells are operated in parallel, different effects such as acoustic interactions, antiresonance, etc. start to occur which should be carefully examined. Depending on the target of operation, 1D or 2D arrays can be used shown in

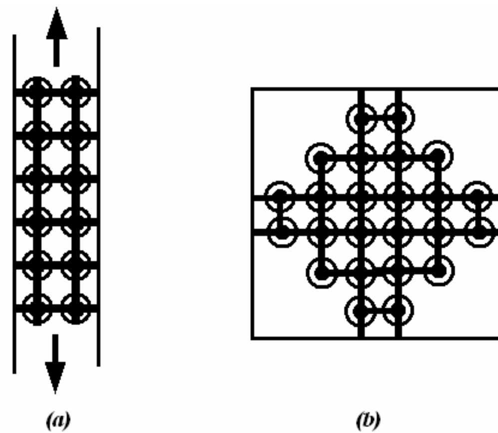

Figure 3.22 : An example of 1D (a) and 2D (b) arrays

When CMUT is operated in an array, the active area becomes very important. The efficiency increases with increased fill factor which is defined as the ratio of the active are to overall device area. If fill factor is low, CMUT elements start to behave individually and lose the efficiency of operation. Moreover, hydrodynamic mass of the

fluid increases and causes a change in the radiation impedance. So there should be a dense design as far as possible to provide a high active area. In order to simulate array operation, 3x3, 4x4 arrays and a hexagonal array of 7 CMUT elements are modeled. Computational time increases as the number of element increases.

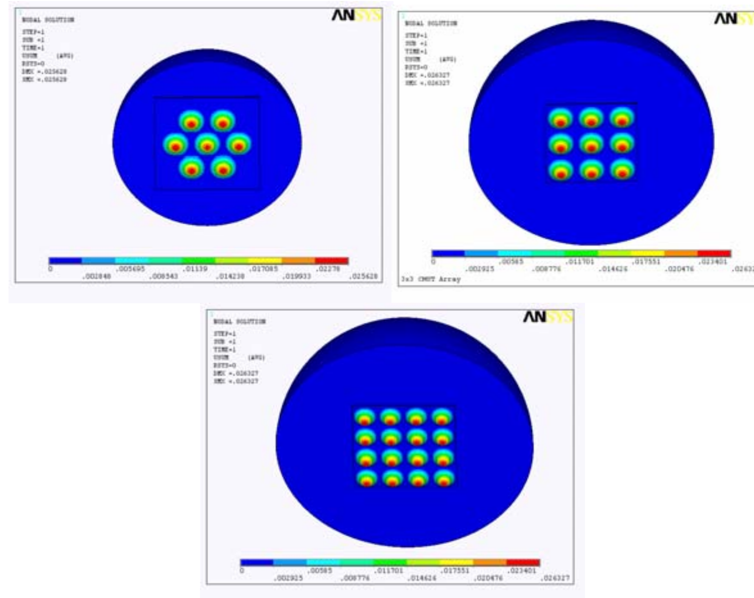

Figure 3.23 : Hexagonal array, 3x3 array and, 4x4 array after a static analysis of 128V DC bias

Transient analysis is done over all three structures. The average pressure over the surface is converted to frequency domain using MATLAB and the results are plotted Figure 3.24. It is found that fractional bandwidth for hexagonal array with 7 elements is 80 percent, for 3x3 array is 100 percent and for 4x4 is 112 percent (Figure 3.25).

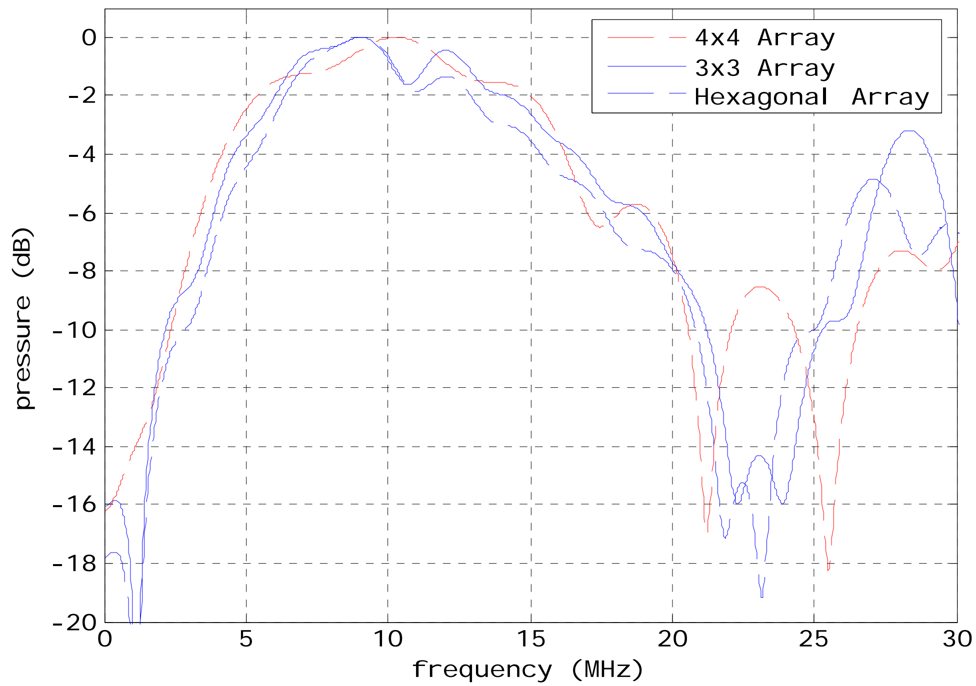

Figure 3.24 : Average pressure over the surface of arrays obtained by using ANSYS

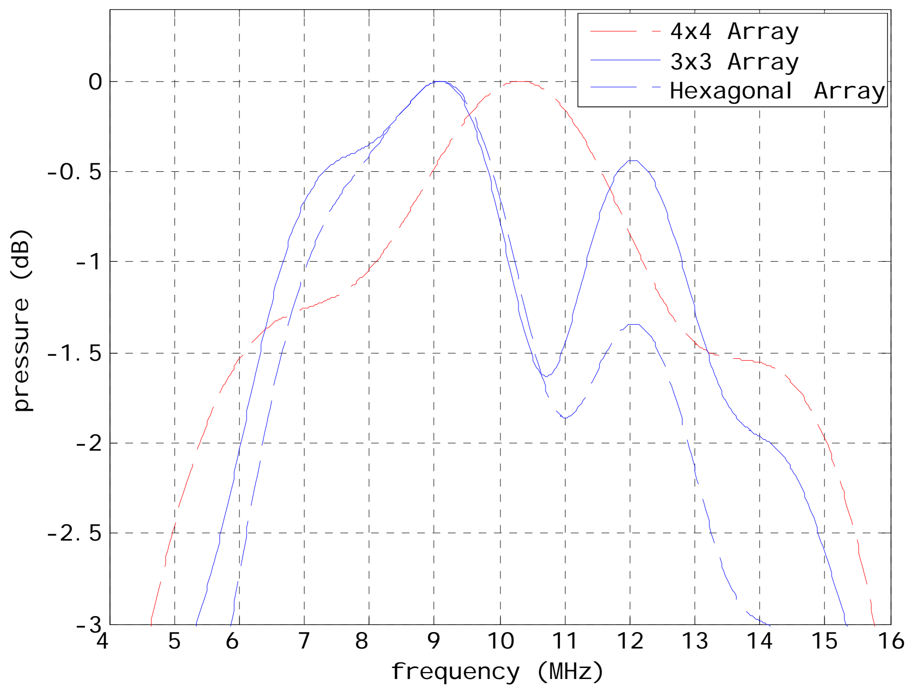

Figure 3.25 : 3dB fractional bandwidth comparison over ANSYS results

CHAPTER 4

MEASUREMENTS

In this chapter CMUT behavior is experimentally inspected. The FEM models described in Chapter 3 have successfully represented the same structure real behavior. It has also been found that transient analysis used in the FEM model gives more accurate results compared to harmonic analysis. Moreover, pulse-echo measurements have been done and CMUT elements are fully characterized.

CMUT arrays with different number of cells are obtained from E. L. Ginzton Laboratory, Stanford. As a comparison with the finite element analysis, 4x4 CMUT arrays are characterized. For an efficient pulse echo measurements 6x6 CMUT arrays are used in experiments.

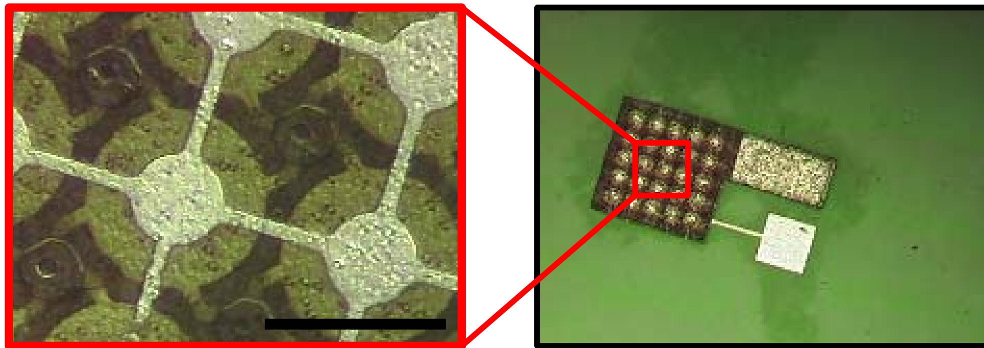

Figure 4.1 : 5x5 CMUT array fabricated using conventional method

Figure 4.1 shows the general structure of the transducer arrays that fabricated using sacrificial layer method. The bottom electrodes of the devices are provided by a metal layer under the active area. And there is no isolation layer over the device surface to allow test setup. The physical parameters of the arrays are given in Figure 4.1. Before the experiments, the transducer arrays are mounted on chip carrier and then wire bonder is used to connect the pads to carrier.

Firstly, impedance measurements are done in air to characterize mechanical and electrical properties of the transducer arrays, as well as the resonant frequency. A

precision impedance analyzer (model 4294A, 40Hz-110 MHz, Agilent) is used to measure electrical input impedance of CMUT arrays in air.

Secondly, transducers are immersed into a vegetable oil for hydrophone measurements to see the generated pressure. The reason using vegetable oil is its very low electrical conductivity which can be used as an isolated environment. The hydrophone (model HGL-200, 0.25 to 40 MHz, Onda Corp.) is placed at a distance of 8mm above the device surface. And CMUTs are driven with a 50 nsec, 10Vp-p pulse generated from a waveform generator (model 33250A, Agilent).

And lastly, pulse echo measurements are done to see device efficiency. Hydrophone and pulse echo measurements are all done using a high sample rate oscilloscope (1GHz,4GSa/s).

Active device area	150μm x 150μm
Bond pad areas	100μm x 100μm
Number of cells	16
Membrane radius	15μm
Membrane thickness	1.2 μm
Gap thickness	0.2 μm
Electrode radius	7.5 μm
Electrode thickness	0.2 μm
Silicon substrate thickness	500 μm
Center to center spacing	5 μm

Table 4.1 : Physical parameters of fabricated CMUT arrays

4.1 Impedance Measurements

When no DC bias is applied to the transducer, the real and imaginary part of the input impedance is found as shown in Figure 4.2. The peak in the impedance curve is detected at 20 MHz which is the resonant frequency of the device. Spring softening effect is observed after applying various DC biases to device and measuring the input impedance simultaneously (Figure 4.3-4.4). A 40V bias shifts the resonant frequency down around 0.9 MHz where the collapse voltage of the device is 160V.

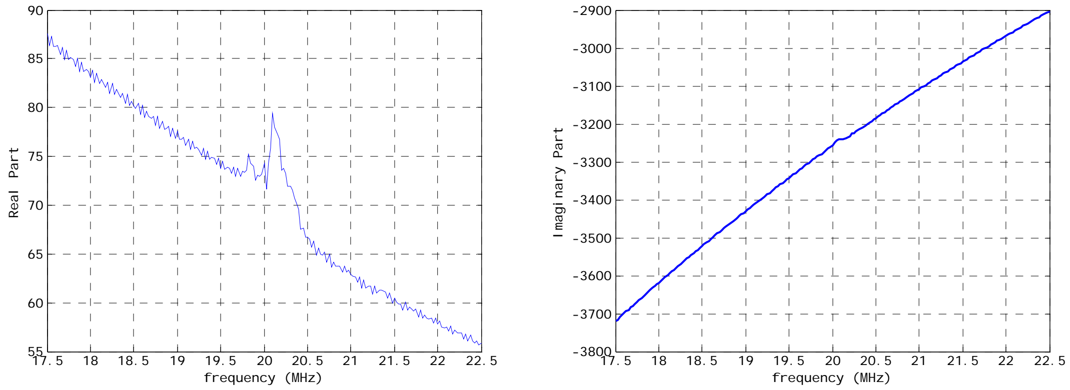

Figure 4.2 : Real and imaginary part of the input impedance of 4x4 CMUT array with no dc bias

Over the frequency range of interest, the imaginary part of the measured input impedance has an impedance characteristic of a capacitance with a mechanical reactance as expected. The behavior can be more easily seen with the increased bias. No zero crossing of the reactive part seen in the measurements compared to simulations. This can be explained with the parasitic capacitance, c_p, in the equivalent circuit model. When there is no parasitic capacitance, short circuit resonance eliminates the device capacitance and there is a zero crossing occur at the reactive part of the impedance curve. But in that case, parasitic capacitance taken from the wire ponds and environment manifests itself when short circuit resonance occurs. Parasitic can also be seen from the change of the flat level of the impedance curves.

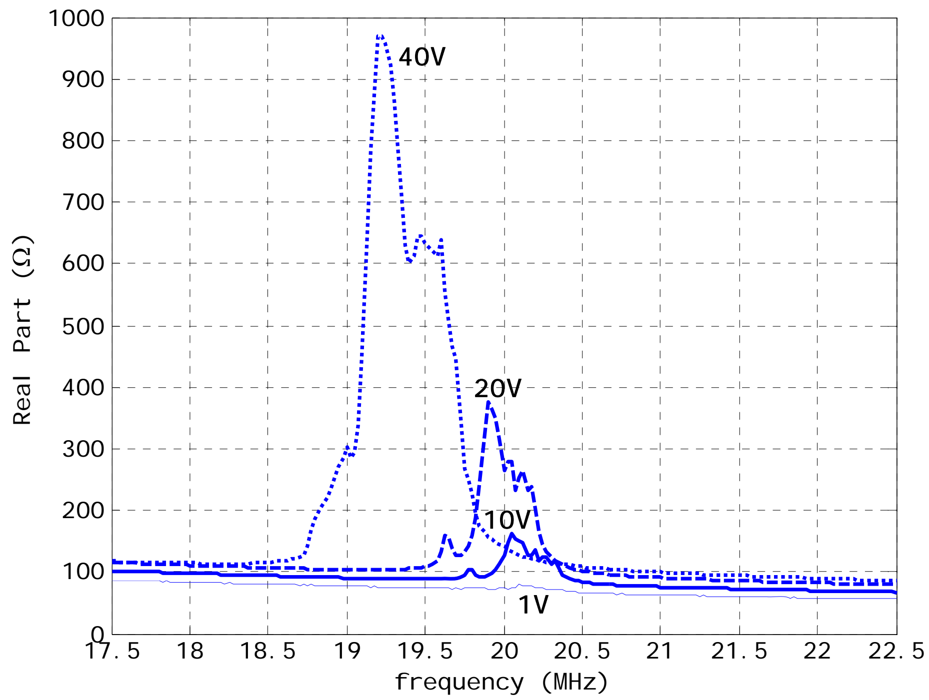

Figure 4.3 : Real part of the input impedance of 4x4 CMUT array at various bias voltages.

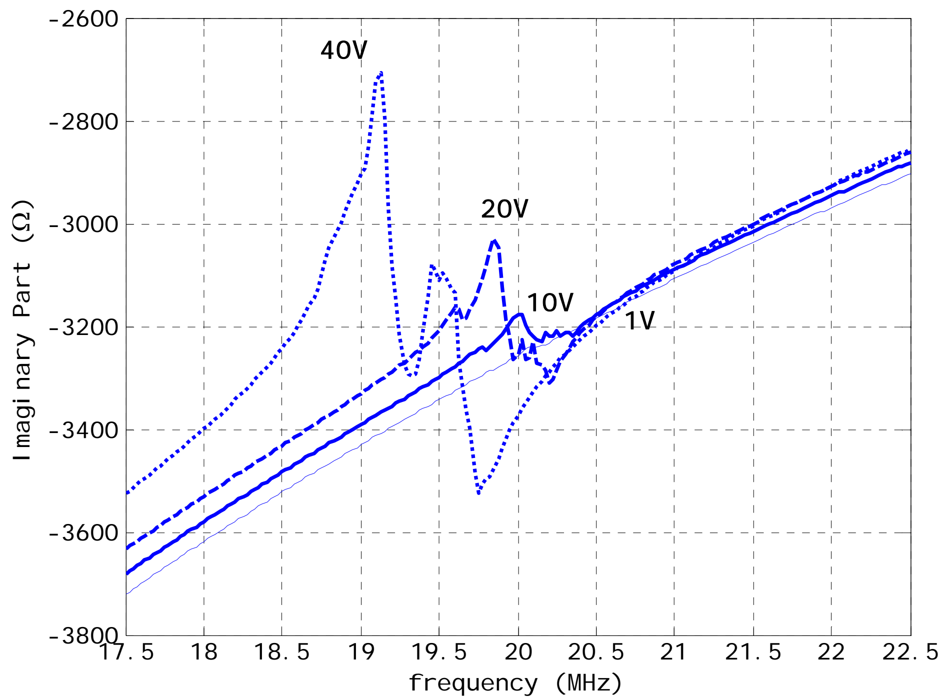

Figure 4.4 : Imaginary part of the input impedance of 4x4 CMUT array at various bias voltages.

Figure 4.5 shows the input capacitance measured from impedance analyzer. The mean capacitance is 2.55 pf with a deviation of 125fF. The calculated capacitance for such bond pads (100µm x 100µm) used for the devices is around 0.615 pF which is a big source of parasitic capacitance [12].

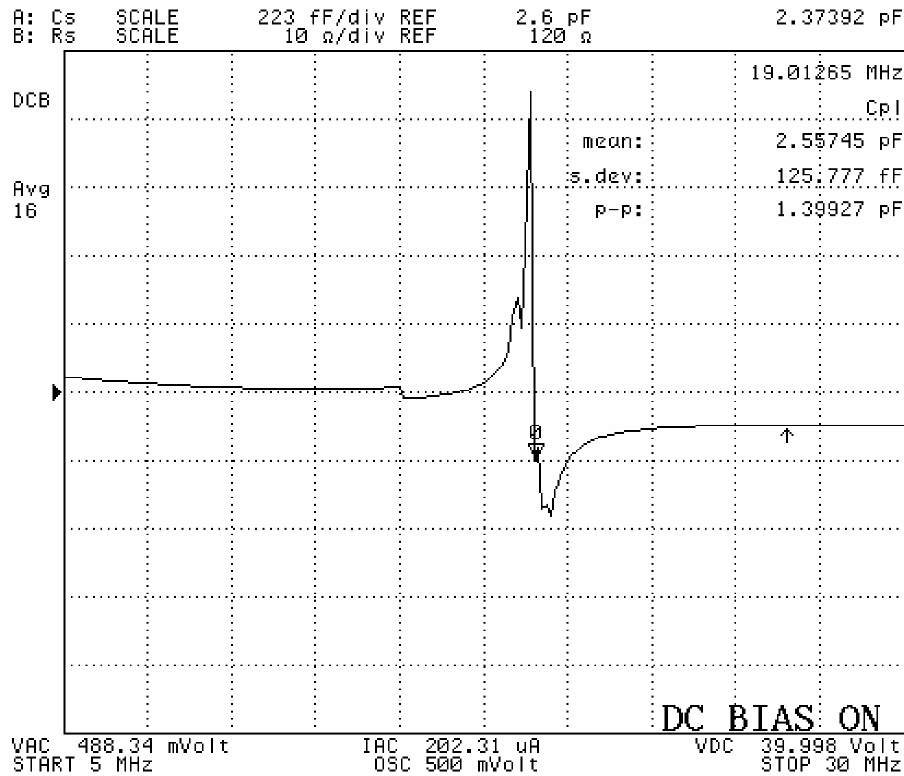

Figure 4.5 : Input capacitance under 30 volt DC bias

4.2 Hydrophone Measurements

In order to characterize the acoustic behavior in terms of pressure, hydrophone measurements are done. The 4x4 CMUT array is dip into a vegetable oil and calibrated hydrophone is placed at a distance of 8mm above the active surface of the device with a minimum acceptance angle. DC bias is set 70 volt and the transducer is driven with a pulse that has amplitude of $10V_{p-p}$ and 50ns width with 1ms repetition rate, the used input signal in experiments is shown in Figure 4.6. The hydrophone amplifier output is directly connected to oscilloscope with 2GSa/s sample rate. Detected pressure signal is averaged 256 times to get a less noised output wave. Figure 4.7 indicates the observed hydrophone data, the pressure wave is received 5.48µs after the applied pulse signal.
The velocity of sound wave in the vegetable oil is found as 1460m/s,

$$v = d / t = \frac{8 \times 10^{-3}}{5.48 \times 10^{-6}} = 1460 \text{ m/s}.$$

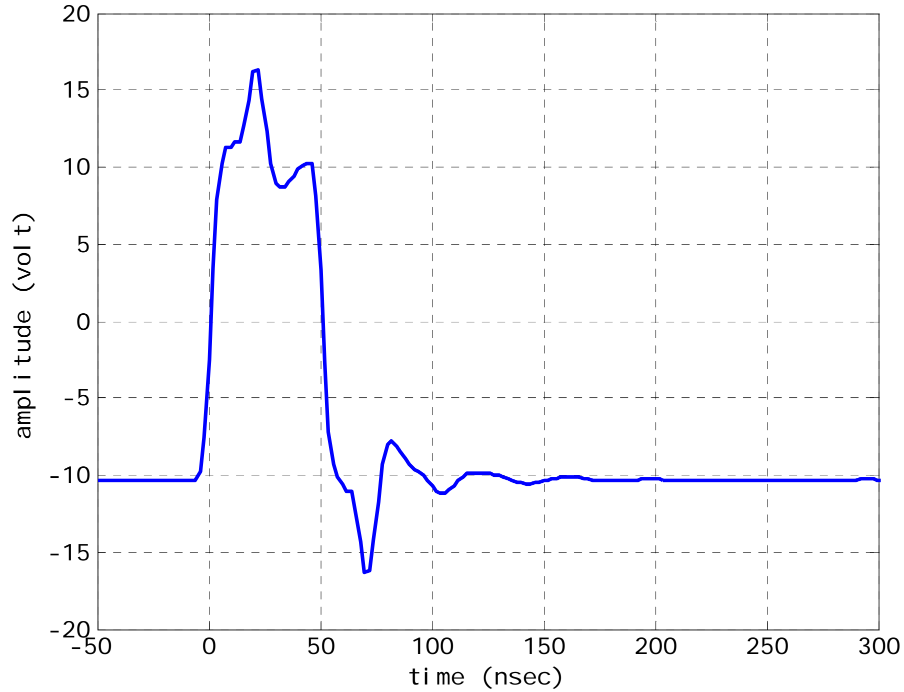

Figure 4.6 : Applied input pulse in the experiments

Detected signal is more apparent in Figure 4.8. The figure also gives the information of the operating frequency of the device in oil where the oscillations occur at 10MHz. The amplitude of the measured signal at the hydrophone output was 4.2 V. When compared to calibration data, the sensitivity of the hydrophone is 44.8 nV/Pa at 10 MHz, so 4.2 mV corresponds to a pressure of 93.75 kPa at 10 MHz at a distance of 8mm. The Fourier transform of the pressure signal is taken to see the frequency response of the pressure wave at the same distance. The observed data is corrected using hydrophone calibration data as displayed in Figure 4.9. The sensitivity of the hydrophone makes a sudden change especially around 9 MHz which falls into the operating frequency range, so the correction should be done. The results are compared to FEM results in terms of pressure bandwidth. A great match is observed with ANSYS simulations and the experiments.

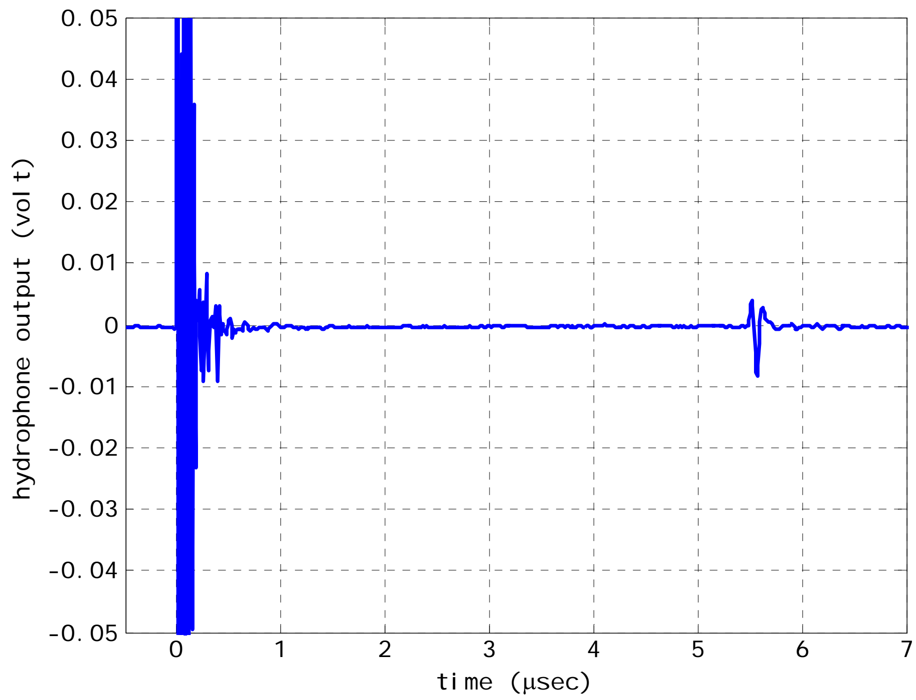

Figure 4.7 : Hydrophone measurement at a distance of 8 mm from the array surface

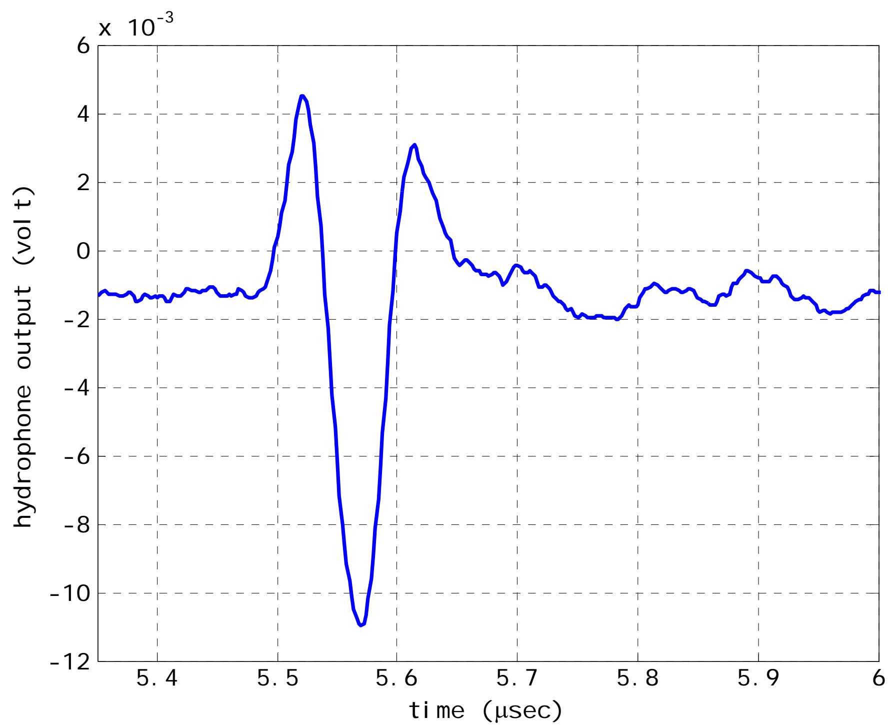

Figure 4.8 : Detected pressure signal at 8mm distance from array surface

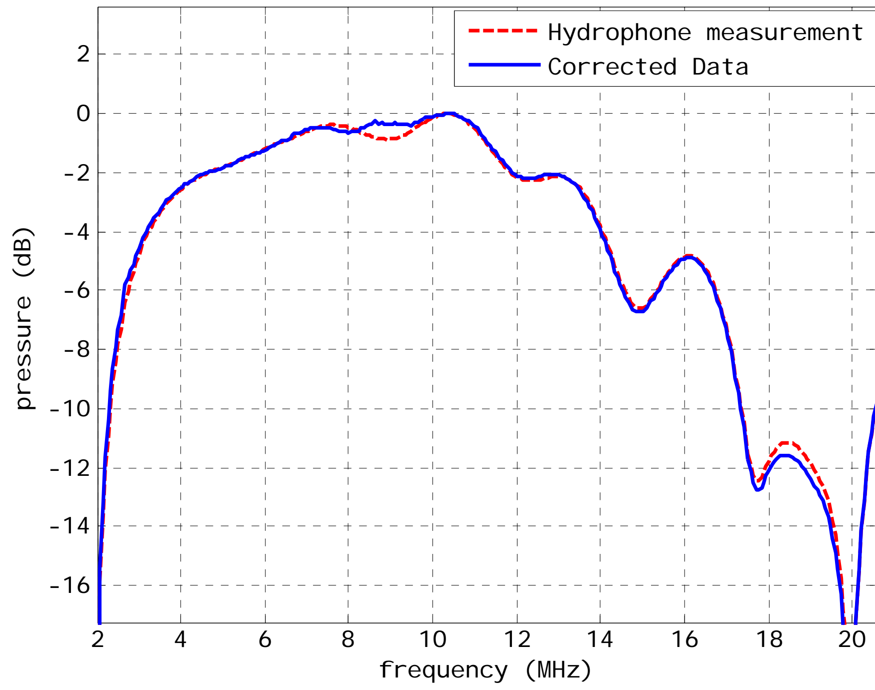

Figure 4.9 : Fourier transform of the detected pressure signal

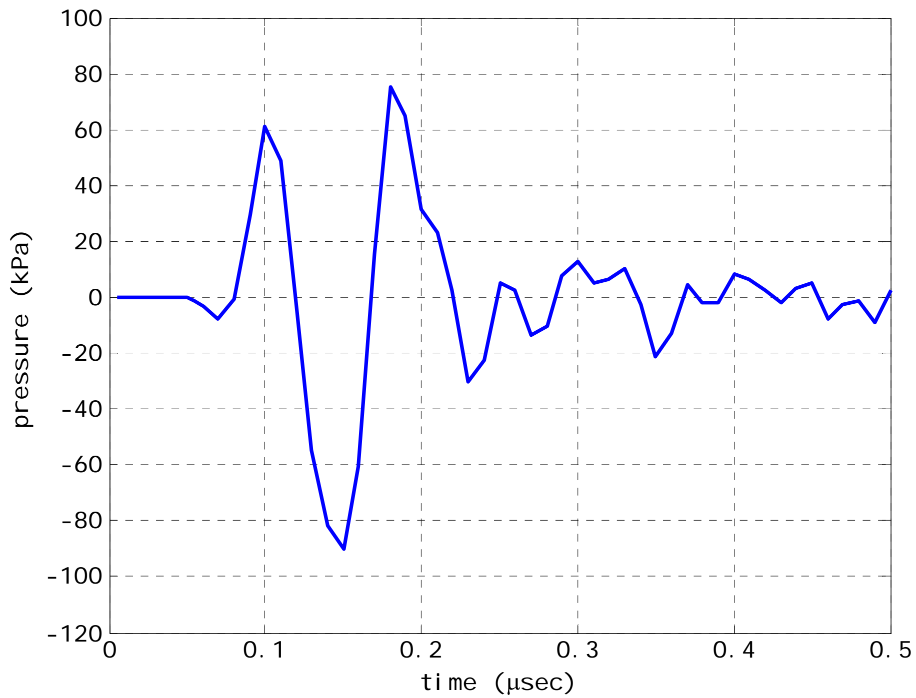

Figure 4.10: Pressure signal at a distance of λ from the transducer surface (FEM). Same pulse signal used as in experimental input.

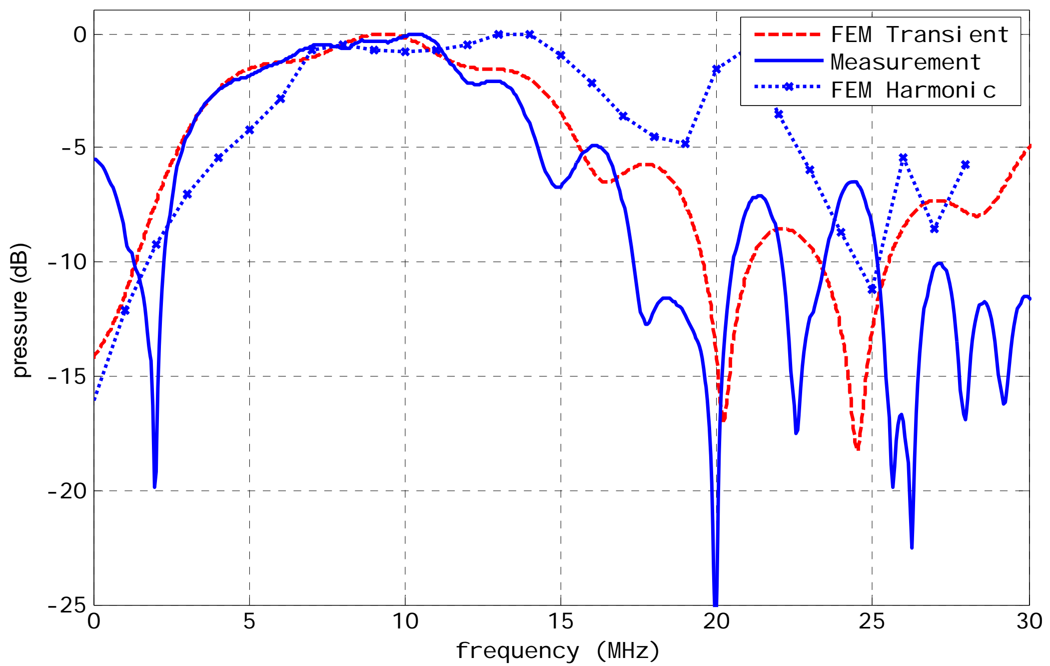

Figure 4.11: FEM analyses results are compared with experimental data in terms of pressure.

Table 4.2 shows ANSYS model properties for 4x4 CMUT element. Transient analysis takes around 4 hours to finalize the simulation with a Pentium IV microprocessor and 2 GB RAM. Harmonic analysis takes around 26 hour to finalize same model. Consequently, transient analysis has a high advantage in process time and accuracy when compared to harmonic analysis.

Element name	Number of elements
SOLID 45	2304
FLUID 30	80448
FLUID 130	6912
TRANS 126	144

Table 4.2 : ANSYS model parameters

4.3 Pulse Echo Measurements

The pulse echo measurements are done with 4 CMUT elements each consist of a 36 CMUT cells to reduce the diffraction and get a higher capacitance change in detection. A flat aluminum block ad a plane reflector is placed to d= 2 mm away from

the CMUT elements. The experimental setup is drawn in Figure 4.12. CMUTs are biased to 70 volt and the same pulse signal is applied as in Figure 4.13.

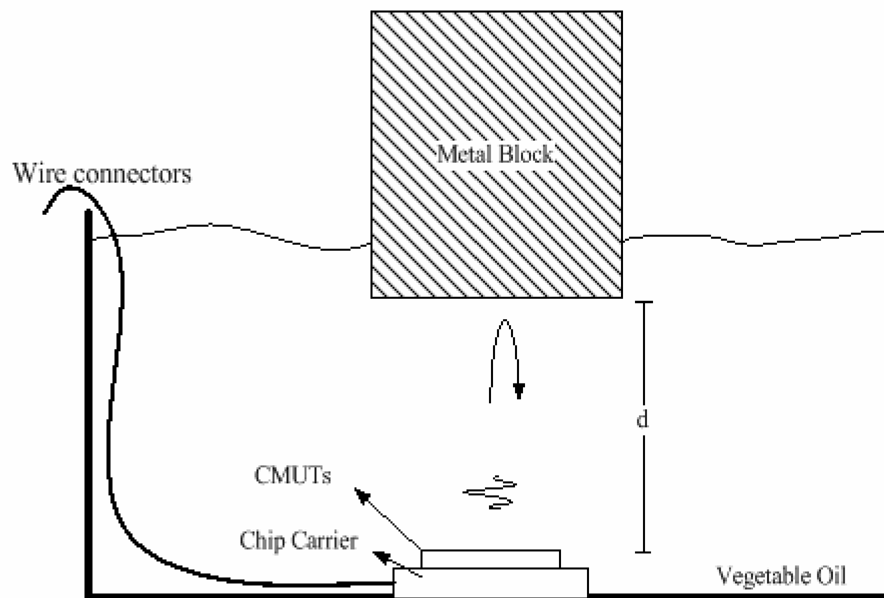

Figure 4.12: Experimental pulse-echo setup

Detection is done over the same CMUT elements. Hence there is no integrated electronics to amplify the return echo signal; the oscilloscope average function is used to eliminate the noise level to see the return echo clearly. Because the signal generator is not ideal and there are no fast switching elements to remove the signal generator from the measurement, the captured echo signal is overlapped to input signal as seen in Figure 4.14. Parasitic capacitance in the measurements is much more compared to transducer capacitance. Figure 4.15 apparently shows the noise level of the return signal compared to echo signal. All that parasitic highly reduces the overall bandwidth up to 20% (Figure 4.16). Absolutely, a much broader bandwidth and improved performance can be obtained using CMUT array with its integrated electronics.

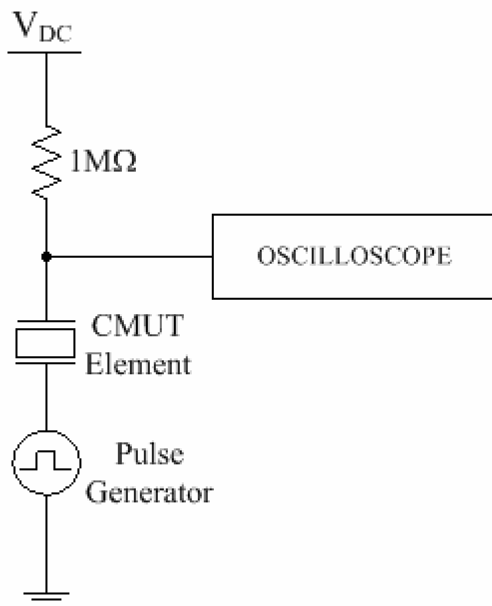

Figure 4.13: Schematic setup for pulse echo measurements.

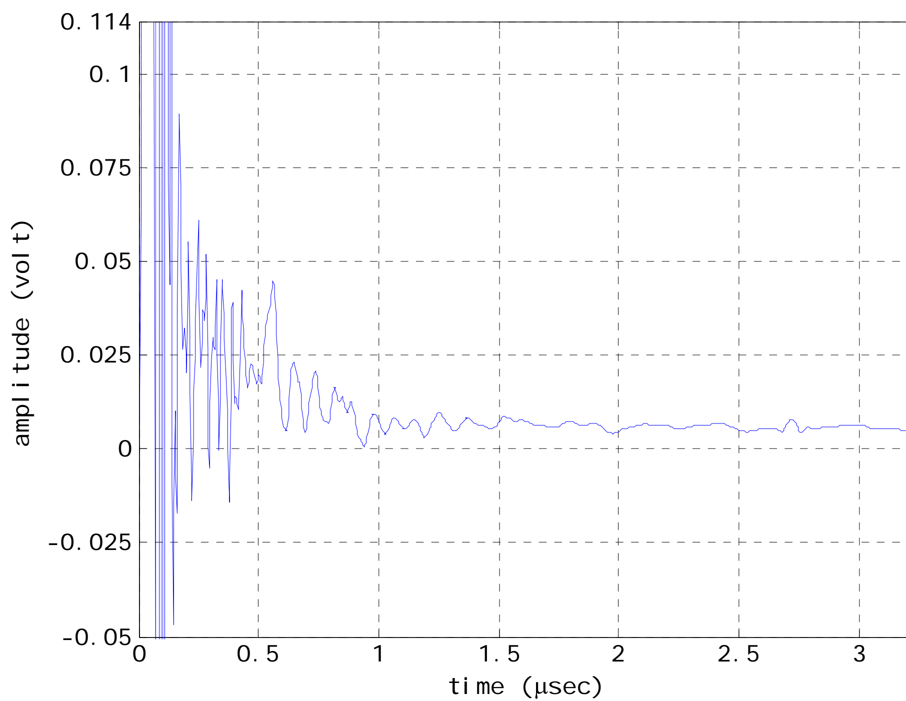

Figure 4.14: Pulse echo response

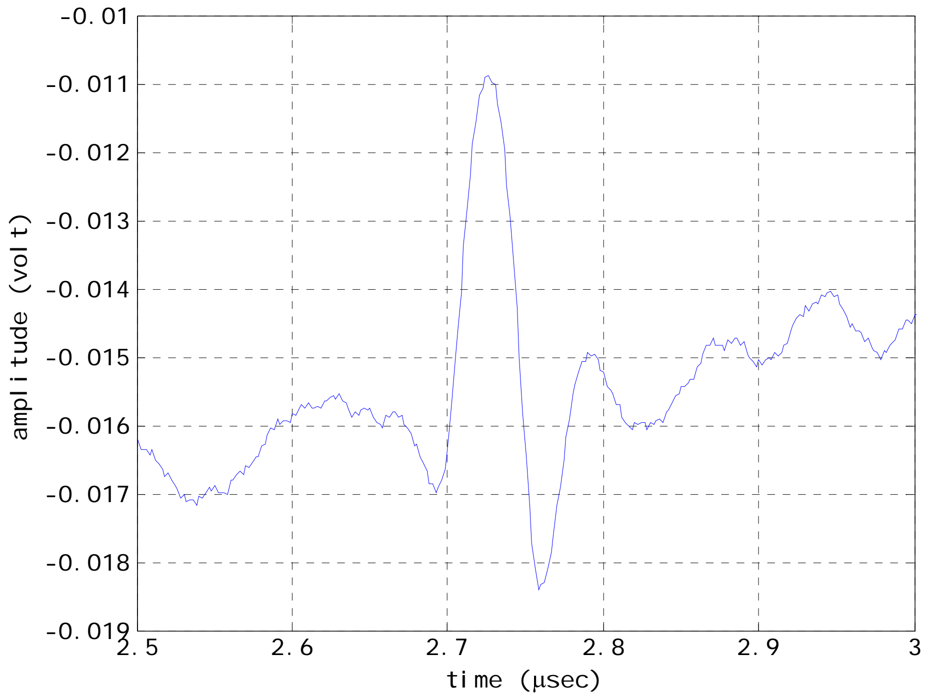

Figure 4.15: Detected echo signal

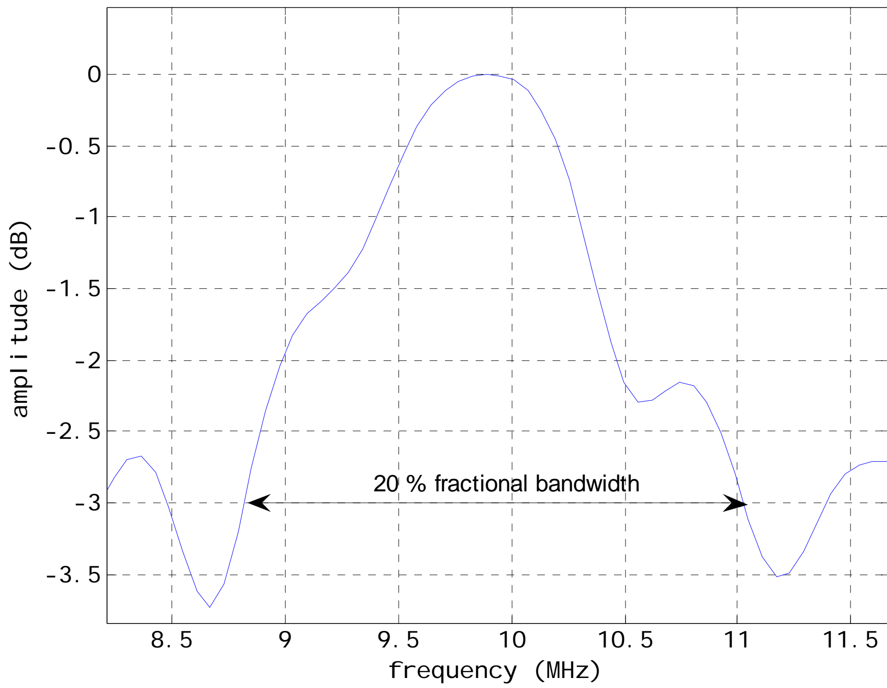

Figure 4.16: Bandwidth of the detected echo signal.

4.4 Equivalent circuit model of the fabricated CMUT element

After proving the FEM performance, the equivalent circuit representation for the device can be done using FEM results. The previously found equivalent circuit model is for a single cell. As the same cells are used in the fabricated CMUT element, the parameters have to be scaled due to parallel operation, except the radiation impedance. From the FEM simulations, it is found that the radiation impedance of each cell is changed due to mutual radiation impedance effects. The overall circuit structure for array operation is illustrated in Figure 4.17.

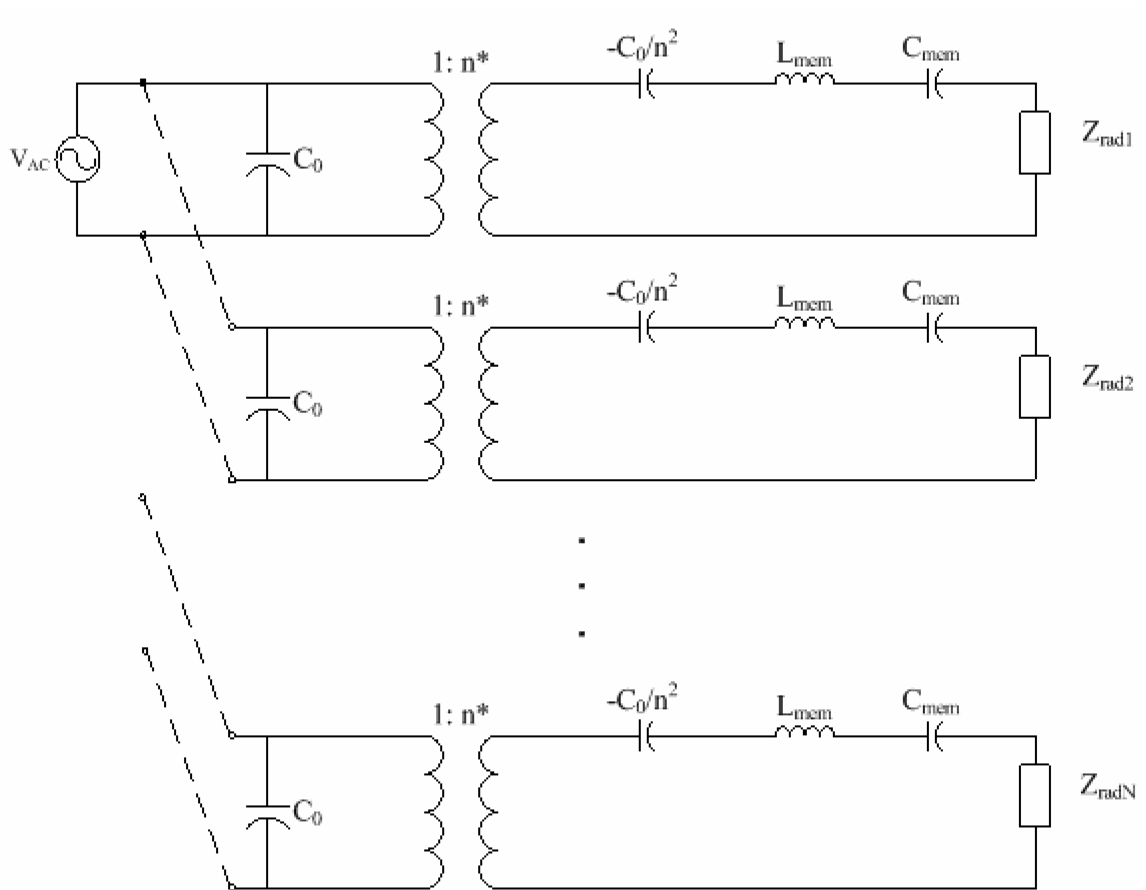

Figure 4.17: Illustration of equivalent circuit model of a CMUT element with N cell.

The radiation impedance value in the new circuit is found using FEM,

$$Z(w) = \frac{\int_{area} P(w).d_{area}}{\overline{v}} \tag{4.1}$$

The pressure integral of the surface nodes of the active device area is divided to the average velocity of the membrane. Corresponding radiation impedance of the overall array is found similar to a single piston transducer with a radius of 60 μm.

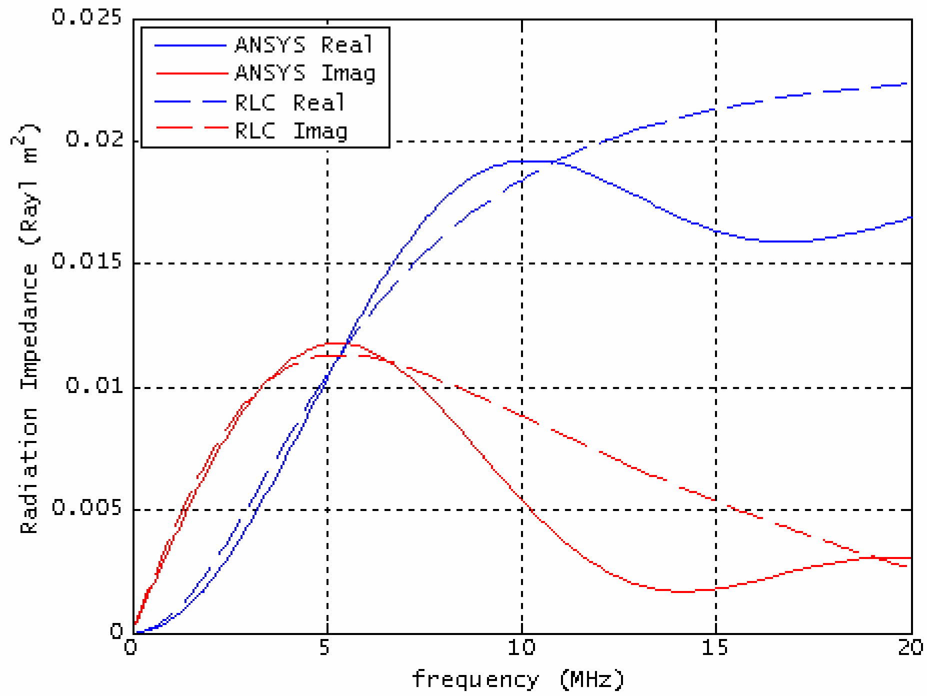

Figure 4.18: Parallel RLC circuit match to the radiation impedance of the CMUT element. Dashed lines show the RLC circuit characteristic.

The RLC parameters that models the radiation impedance, is found as 22.6mΩ, 33.2pH and 57.6nF respectively. The circuit models the radiation impedance in good accuracy especially in low frequencies (Figure 4.18).

Obviously, device capacitance will be equal to N times C_0 and membrane mechanical impedance will be divided N due to parallel combination in the equivalent model.

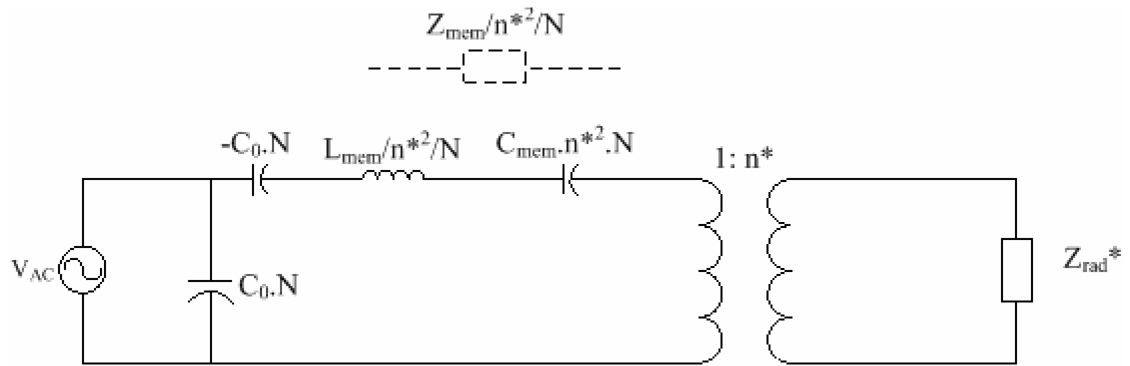

Figure 4.19: Equivalent circuit representation of the CMUT element with N cell

In Figure 4.19 the equivalent circuit for the element is shown in a different point of view. The membrane mechanical impedance is transferred to the electrical domain with the spring softening capacitance, so the radiation impedance is only left at the mechanical domain. The circuit with equivalent component values is given in Figure 4.20.

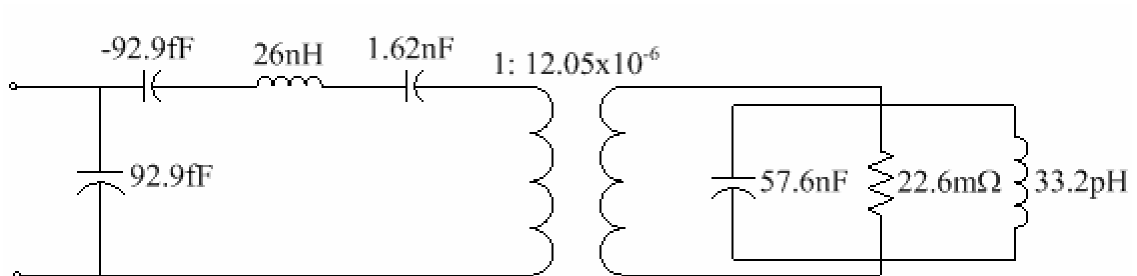

Figure 4.20: Obtained equivalent circuit model of the CMUT element used in experiments.

The input impedance of the device is plotted with ANSYS results between 1-30 MHz as shown in Figure 4.21.

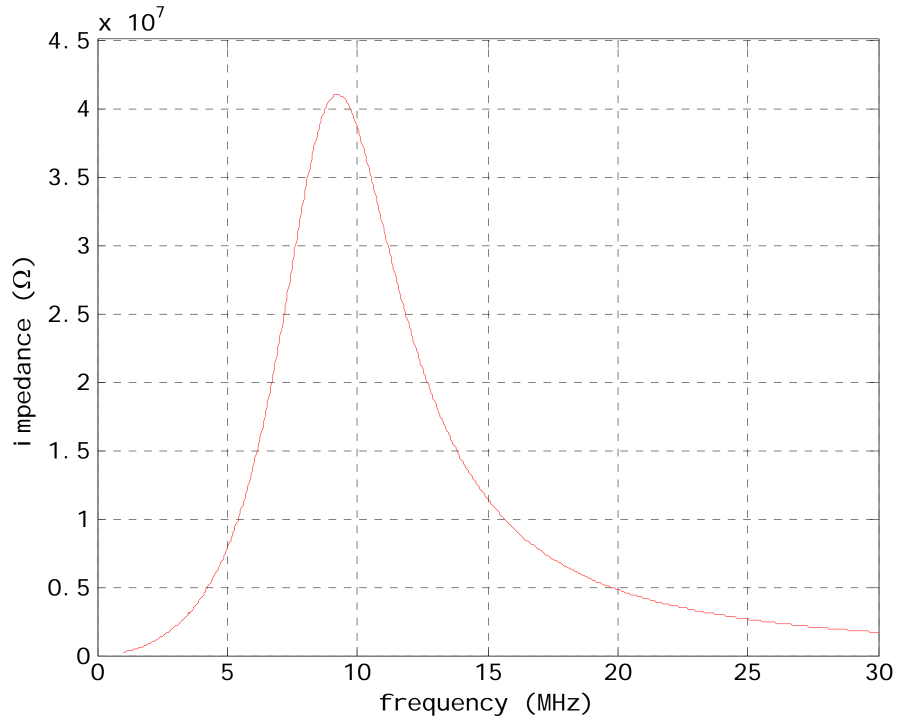

Figure 4.21: Input impedance comparison between equivalent circuit and ANSYS results for the CMUT element consists of 16 cells.

CHAPTER 5

CONCLUSION AND FUTURE WORK

In this thesis, we have demonstrated a comprehensive FEM model of CMUT. The developed FEM model results are match to experimental result with a high accuracy. It is found that transient analysis is a more effective solution to see the device bandwidth. Corresponding equivalent circuit parameters extracted from the FEM are also predicted the CMUT behavior in electrical ports. The mason model parameters are modified through the FEM results. The equivalent circuit model still needs more components to properly operation. The matched RLC circuit requires to be improved by adding more electrical components to the radiation impedance part. The future work will be on modeling the mutual impedance between the individual cells of an element to get more precise results from the equivalent circuit model. Also, parasitic capacitance effects are neglected in our model but have a high effect on the transducer efficiency. By including all the effects a pulse echo model is aimed which can be than used in transceiver circuit designs.

A part of this work is presented in 5th International Micromachined Ultrasonic Transducer (MUT) Workshop in Munich.

BIBLIOGRAPHY

[1] Igal Ladabaum, X.J., Hyongsok T. Soh, Abdullah Atalar, and Butrus T. Khuri-Yakub, *Surface Micromachined Ultrasonic Transducers.* IEEE Trans. Ultrason., Ferroelect., Freq. Contr., 1998. 45(3): p. 678-690.

[2] Arif Sanlı Ergun, Y.H., Xuefeng Zhuang, Omer Oralkan, Goksen G. Yaralioglu, Butrus T. Khuri-Yakub, *Capacitive Micromachined Ultrasonic Transducers: Fabrication Technology.* IEEE Trans. Ultrason., Ferroelect., Freq. Contr., 2005. 52(12): p. 2242-2258.

[3] H. Jagannathan, G.G.Y., A.S. Ergun, F.L. Degertekin, and B.T. Khuri-Yakub, *Micro-Fluidic Channels with Integrated Ultrasonic Transducers.* IEE Ultrasonic Symposium, 2001: p. 859-862.

[4] Ömer Oralkan, S.T.H., Barış Bayram, Göksen G. Yaralıoğlu, A. Sanlı Ergun, and Butrus T. Khuri-Yakub, *High-Frequency CMUT Arrays for High-Resolution Medical Imaging.* IEEE Ultrasonics Symposium, 2004.

[5] Ömer Oralkan, A.S.E., Jeremy A. Johnson, Mustafa Karaman, Utkan Demirci, Kambiz Kaviani, Thomas H. Lee and Butrus T. Khuri-Yakub, *Capacitive Micromachined Ultrasonic Transducers: Next-Generation Arrays for Acoustic Imaging?* IEEE Trans. Ultrason., Ferroelect., Freq. Contr., 2002. 49(11): p. 1596-1609.

[6] Joshua Knight, J.M., and F. Levent Degertekin, *Low Temperature Fabrication of Immersion Capacitive Micromachined Ultrasonic Transducers on Silicon and Dielectric Substrates.* IEEE Trans. Ultrason., Ferroelect., Freq. Contr., 2004. 51(10): p. 1324-1333.

[7] Badi, M.H., *Capacitive Micromachined Ultrasonic Lamb Wave Transducers*. 2004, Stanford University.

[8] A. Bozkurt, I.L., A. Atalar, B. T. Khuri-Yakub, *Theory and analysis of electrode size optimization for capacitive micromachined ultrasonic transducers.* IEEE Trans. Ultrason., Ferroelect., Freq. Contr., 1999. 46(6): p. 1364-1374.

[9] Yaralioglu G., E.A., Bayram B, Marentis T., Khuri-Yakub B.T., *Residual Stress and Young Modulus Measurement of Capacitive Micromachined Ultrasonic Transducer Membranes.* Ultrasonic Symposium, 2001.

[10] Goksen G. Yaraliogli, M.H.B., A. Sanli Ergun, and Butrus T. Khuri-Yakub, *Improved Equivalent Circuit and Finite Element Method Modelling of Capacitive Micromachined Ultrasonic Transducers.* IEEE Ultrasonics Symposium, 2003.

[11] *ANSYS Element Reference*. ANSYS Release 6.1 Documentation.

[12] Utkan Demirci, A.S.E., Omer Oralkan, Mustafa Karaman,and Butrus T. Khuri-Yakub, *Forward-Viewing CMUT Arrays for Medical Imaging*. IEEE Trans. Ultrason., Ferroelect., Freq. Contr., 2004. 51(7): p. 886-893.

[13] B Belgacem, D.A., P Muralt, J Baborowski, S Lucas and R Jerisian, *Optimization of the fabrication of sealed capacitive transducers using surface micromachining*. Journal of Micromechanics and Microengineering, 2003: p. 299-304.

[14] Xuecheng Jin, L., I., Degertekin, F.L., Calmes, S., Khuri-Yakub, B.T., *Fabrication and Characterization of Surface Micromachined Capacitive Ultrasonic Immersion Transducers.* Journal of Microelectromechanical Systems, 1999. 8(1): p. 110-114.

[15] Yongli Huang, A.S.E., Edward Hæggström, Mohammed H. Badi, and B. T. Khuri-Yakub, *Fabricating Capacitive Micromachined Ultrasonic Transducers With Wafer-Bonding Technology.* Journal of Microelectromechanical Systems, 2003.

[16] Auberton-Herve, S.S.l.a.A.J., *Silicon Wafer Bonding Technology for VLSI and MEMS Applications*. EMIS. 2002, Unighted Kingdom: INSPEC.

APPENDIX A

FABRICATION OF CMUTs

CMUT technology is prime candidate for next generation imaging systems. Formerly, the interest in CMUTs was for airborne applications such as non-destructive evaluation (NDE), mainly because the cavity could not be sealed at the time. After the techniques were developed to seal the cavity, application areas of the device were increased and started to use in the field of underwater imaging and medical imaging.

The first CMUTs were formed using a sacrificial release process which has become the standard CMUT fabrication method. Numberless variations of the method have been published and, all based on the same principle. The cavity under the membrane is created by depositing or growing a sacrificial layer on the substrate, especially chosen to etch the sacrificial material not to etch the membrane material. Even the method does not change so much, different materials used as in the process.

Process temperature is the fundamental parameter that determines whether CMUTs can be fabricated on the same wafer with electronics. If the CMUTs are constructed on the same silicon wafer with the CMOS electronic circuitry, the highest temperature in overall process cannot exceed 400^0 C in which the process is called CMOS compatible. And the others are simply called high temperature processes.

A.1 Conventional Method: Sacrificial Layer

Even this process has a long past, still it is preferred to achive a low cost device fabrication. It has lots of disadvantages compared to wafer bonding method such as non uniform cavities, stressed membranes, too many mask requirement etc. Wafer bonding method is still under investigation, so once a while sacrificial method will be used. Figure A.1 illustrates overall process. The sacrificial layer method begins with an electrically conductive silicon wafer. The silicon wafer is doped to accomplish a high conductive layer over the surface which serves as the bottom electrode of the CMUT.

The disadvantage of the case is, all moving parts of the top electrode act as a

parasitic capacitance. An illustration of sacrificial etch-release process with substrate bottom electrode is shown in Figure A.1. To solve this problem a thin metal layer can be deposited over the substrate and patterned. Then, a thin silicon nitride layer is deposited to protect the surface for further sacrificial etch process. This layer is also called the etch-stop layer. It should be thick enough to protect the silicon or metal surface during long, wet chemical etch, besides it should not be arbitrary thick to avoid the decrease of device active capacitance. Typically it is around 100 nm thick[2].

Poly-silicon is a common sacrificial material with high etch selectivity to silicon nitride. It can be patterned with a reactive ion etch (RIE). Also different type of metals can be used as sacrifical layer. For lower gap heights, chromium is found to be a good choice, hence it does not oxidize and easily removed with commercially available wet enchants. After the patterning, first silicon nitride layer is deposited. The thickness of this layer must be high to prevent sticktion problem arising from drying of the wafer after the removal of sacrificial layer. This produces capillary forces, which stick the bendable structure to the substrate, rendering the device useless. The easiest way to avoid that situation, a high, thick layer is deposited and then the sacrificial layer is removed. After the process finished, desired thickness can be observed with etching and thinning the membrane. Next, holes are formed over the silicon nitride layer using dry etch. CHF_3 gas is used to etch silicon nitride down to sacrificial layer.

Potassium hydroxide (KOH) is generally used for removing poly-silicon. It has a temperature dependent etch rate. However, etch selectivity of KOH gets worse at high temperatures. To form a uniform gap structure, long etch time is preferred. During the etching, etch stop layer prevents the silicon substrate or bottom electrode. Figure A.1 illustrates overall process.

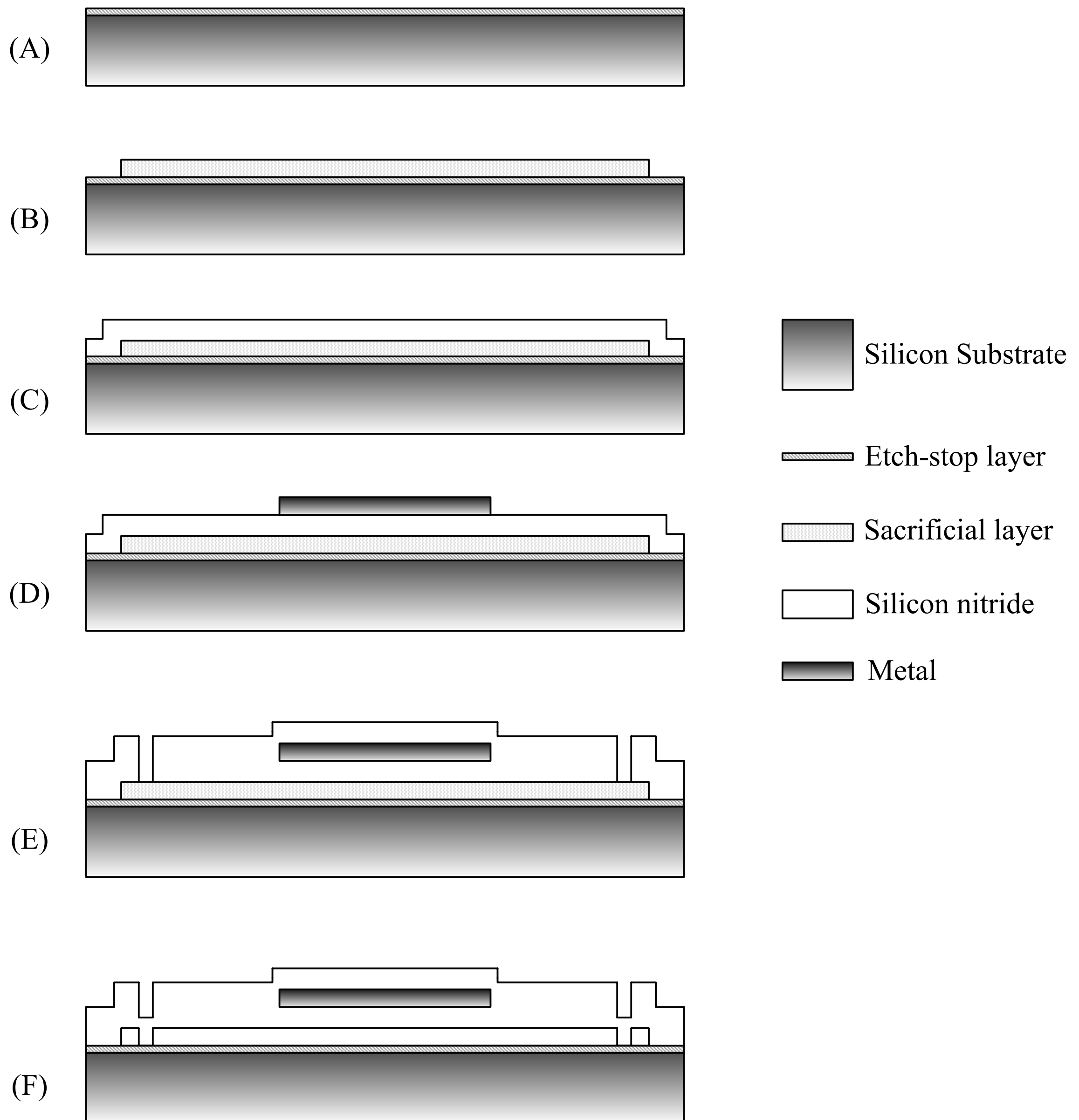

Figure A.1 : Illustration of sacrificial layer method

A.1.1 Vacuum Sealing

When using a transducer in immersion, it is necessary to seal the openings which are used to etch sacrificial layer. Sealing reduces the loss caused by the trapped air/liquid inside the cavity.

Due to the high electric field presented when the electrodes are biased vacuum sealing is required in order to reduce the break phenomena in air inside the cavity.

Furthermore, the vacuum sealing of cMUT is required to obtain better sensitivity. Before the deposition of sealing materials it is important to obtain a low pressure inside the deposition chamber[13].

A.1.2 Metallization

The transducer metallization can be examined in two parts: the electrodes just above the cavity, and the interconnects which bridges adjacent cells together. Due to parasitic capacitance, less metallization area is always preferred. Finite element analysis shows that a properly sized top electrode provides better efficiency and, increases bandwidth. The narrow interconnect reduces the parasitic capacitance, but it also gives higher resistance between cell elements reduce the CMUT performance. It has three reasons: higher loss due to the higher serial resistance; higher noise level due to the increased transducer impedance; and efficiency drop due to the phase shift through cell elements. Likewise, thin metallization layer yields easier and composes less stress perturbation on the membrane, on the other hand it increases the resistance between CMUT cells [14].

A.2 Wafer Bonding Method

CMUT fabrication with wafer bonding method has many advantages over conventional method. It simplifies the fabrication process especially by eliminating the sealing step in the conventional method. It reduces the number of process steps as well as provides solutions for many of the limitation problems. In the wafer-bonding technique, the membrane and the cavity are formed on separate wafers that are later bonded under vacuum conditions. This process provides more control over the gap height and flatness. Likewise membrane thickness is more accurate while it is grown of the handle substrate in a single step. When a single crystal material is transferred as a membrane then residual stress effect is also discouraged.   Even though it is an improvement in the process, it is expensive due to SOI wafer usage.

A.2.1 Vacuum Cavity Formation

With wafer bonding, it is easier and faster to form a vacuum cavity than it is with the surface micromachining process. The new technique has a primacy, discarding the sealing process with its complex via open and refill process. Wafer bonding also avoids adding unwanted material, such as SiO_2 or Si_3N_4, onto the membrane's inner surface during the via refill process. This should result in higher thickness uniformity across individual membranes and in higher thickness conformity between the membranes in a device.

A.2.2 Cavity Size and Shape

In wafer bonding technique, the cavity shape is independent from the membrane shape. The design parameters such as height, shape, size of the gap and membrane can be easily optimized. The process does not deal with longer etch times of sacrificial layer and aspect ratio problems. And, due there is no unwanted material deposition inside surfaces of the gap the uniformity of the cavity does not change which means a better control over the operating voltage [14].

A.2.3 Membrane Material

The membrane is made from single crystal silicon, which has desirable mechanical properties, e.g., few internal defects, low internal mechanical loss, and very low internal stress. This will improve the device reliability, especially important with large devices with hundreds of membranes, as well as the performance of the device. By using an SOI wafer to form the membrane, one can achieve a good thickness uniformity of the membrane.

A.2.4 Fill Factor

There is no need to form the complex etch channels as in conventional method. The area occupied by these channels can be partially utilized as active transducer area in the wafer-bonded CMUT (73% active area compared to 56%, with 12 μm membrane and 2 μm post width)[15]. This effect is more pronounced when fabricating high-frequency devices featuring small membranes each of which requires these channel structures.

A.2.5 Fabrication Process

Fabricating CMUTs by the wafer-bonding technique is a four-mask process as shown in Figure A.2. The process starts with a low resistivity, 0.008–0.02 Ω/square, 4-in N-type silicon <100> wafer that will be used as bottom electrode. The first step (Figure A.2.A) is to grow silicon dioxide at around 1100° C on the silicon wafer prior to cavity definition. Cavity can be formed only etching the oxide layer. If this depth is not enough for the cavity, then a second etch process is done to etch the silicon substrate. In the first etch, the oxide layer is patterned with photolithography and etched with buffered oxide etch (6:1 BOE) that stops on the silicon surface. Therefore, the cavity depth is determined by the thickness of the oxide layer. After photoresist removal, another thermal oxide layer is grown as an electrical isolation layer for the CMUT. For the second etch process, potassium hydroxide (KOH) at 70° C or dry etch with sulphur hexafluoride (SF6) can be used to make a deeper cavity. After the creation of cavity, the wafer is ready for bonding (Figure A.2 B). The surface uniformity and cleanliness is extremely important for wafer bonding. Therefore, prior to the bonding, the wafer surface is cleaned and activated; first, in Piranha (4:1 Sulfuric Acid: Hydrogen Peroxide) for 20 min, then in 50:1 hydrofluoric acid (HF) for 15 seconds. Finally, the wafer surfaces are treated in RCA1 (H_2O:H_2O_2:NH_4OH = 5:1:0.2-1) for 5 min to obtain a hydrophilic surface. Primarily, the wafer bonding is done with a bonder at mbar vacuum level, at a temperature of 150° C (Figure A.2. C). The bonded wafers are then annealed at 1100 C for two hours to make a strong bond. Bonding energy versus temperature and annealing time is shown in Figure A.3. After this, the wafers are ground and etched back (using KOH) to the box (oxide layer) of the SOI wafer to form the membrane (Figure A.2 D).

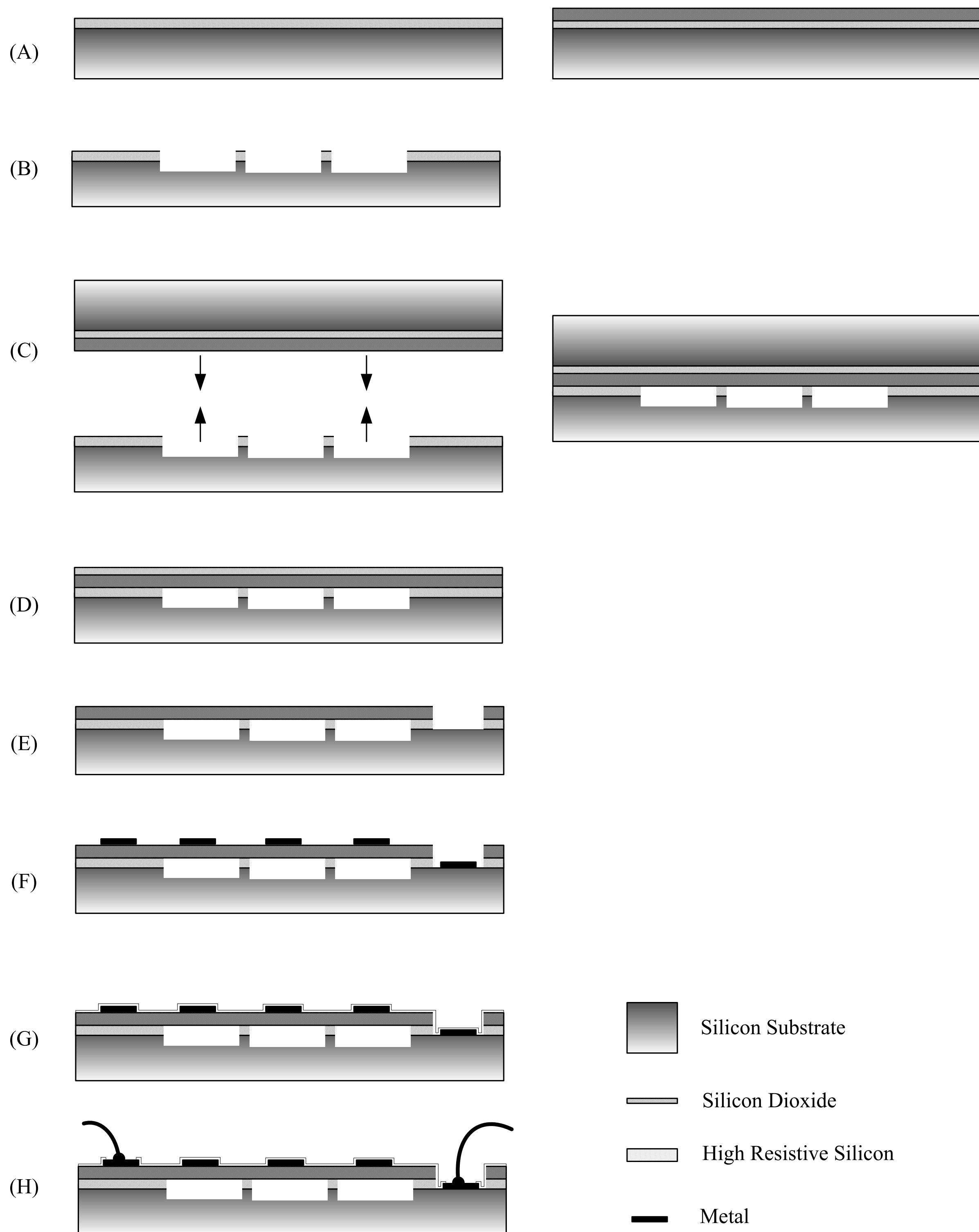

Figure A.2 : Illustration of wafer bonding method. Thermal oxidized silicon substrate and SOI wafer (A). thermal oxide and silicon etch respectively to form the cavity (B). Silicon wafer fusion bond (C). Ground etch back and remove the box (D). Metal deposition and patterning (E). Thin oxide or nidride deposition as passivation layer and patterning (F). Wire bond to electrodes (G).

The box layer is removed with the same BOE solution. This completes the membrane fabrication. In order to be sure that bonding occurs on intermediate surface, the thin membranes are allowed to be pushed by the atmospheric pressure toward the posts and a postanneal is performed to improve the bond between the membrane and the posts. The active silicon layer is subsequently patterned by photolithography and plasma etching (Figure A.2 E). One purpose of the etching is to open a via through the top layers to contact the bottom electrode of the CMUT. Another purpose is to make an isolation trench between CMUT arrays. After this, gold or aluminium is sputtered by a metal sputter system and patterned to serve as the top electrode for the CMUT (Figure A.2 F). The sputtering is followed by a passivation step where a thin low temperature oxide (LTO) is generated (Figure A.2 G). Then, the LTO layer is patterned to open pads for wire bonds (Figure A.2 H).

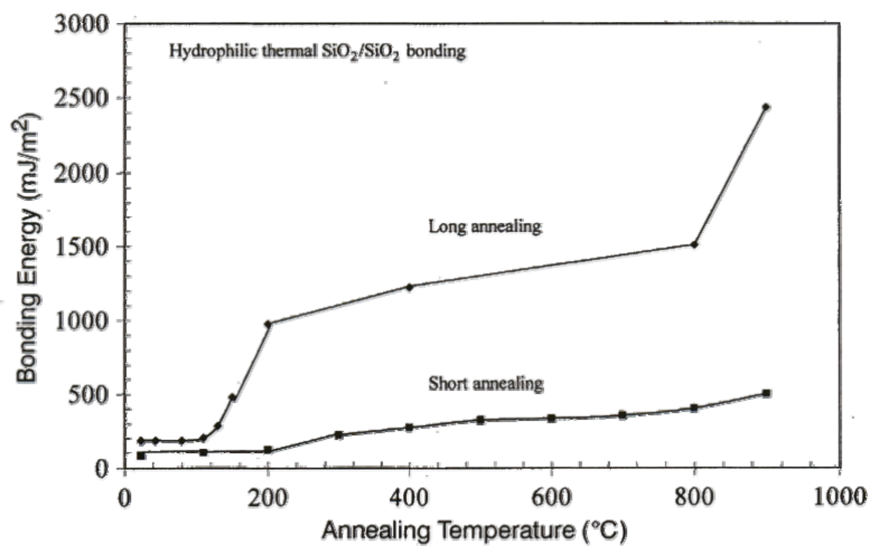

Figure A.3 : Bonding energy of typical bonded hydrophilic oxidized silicon wafers as a function of annealing temperature. Both short and long annealing cases are shown [16].